

Project No. 09-766

Improved LWR Cladding Performance by EPD Surface Modification Technique

Integrated University Programs

Dr. Michael Corradini
University of Wisconsin, Madison

Steve Marschman, Technical POC
Frank Goldner, Federal POC

FINAL REPORT

Project Title: Improved LWR Cladding Performance by EPD Surface Modification Technique

Covering Period Nov 1, 2009 to Oct 30, 2012

Date of Report: November 30, 2012

Recipient: University of Wisconsin – Madison

Department of Engineering Physics 1500 Engineering Drive Madison, WI, 53706

6.0 – Investigator Initiated Research

Principal Investigators:

Project Number: 9-766

Michael Corradini (608-263-1648): Corradini@engr.wisc.edu

Kumar Sridharan (608-263-4789): kumar@engr.wisc.edu

Objectives: UW-Madison researchers utilized the Electrophoretic Deposition technique (EPD) in conjunction with nanoparticles to deposit oxide coatings on prototypic zirconium-alloy cladding surfaces. After demonstrating that this surface modification was reproducible and robust, we subjected the modified surface to boiling and corrosion tests to characterize the expected improvements in nucleate boiling behavior and associated corrosion performance. We have divided the scope of work into three tasks:

- Surface Modification of Metal Alloy Cladding Samples with Nanoparticles
- Pool Boiling Tests with Metal Samples to Characterize CHF Performance
- Corrosion Tests with Cladding Samples with Nanostructured-surface

Our final report is divided into three separate sections on [1] Description of the EPD technique and initial pool boiling experiments, [2] Detailed pool boiling studies that identifies the beneficial effects of EPD surface modifications and [3] Corrosion testing and initial results.

1.0 EPD Nanoparticle Surface Modification Effects on Pool Boiling Critical Heat Flux

Executive Summary

Pool boiling critical heat flux (CHF) measurements have been performed on stainless steel and zirconium wires in nanofluids consisting of oxide nanoparticles (7 to 250nm) dispersed in water as well as in high purity water after coating these wires with a variety of materials and methods. For the nanofluids study, nanoparticles of titania, alumina, zirconia, and yttria-stabilized zirconia (YSZ) were investigated for various sizes and concentrations. Results showed improvements in CHF in the range of 50% to 100%, with titania exhibiting the highest improvements and zirconia yielding the lowest levels of improvement. Wires were coated separately with the same oxide nanoparticle materials, as well as pure titanium nanoparticles, using the electrophoretic deposition (EPD) process and by nanofluid boiling. EPD coatings yielded superior and more consistent improvements in CHF values in clean water, suggesting that this could be a more practical approach than using nanofluids. Coating uniformity plays an important role in dictating the levels of CHF enhancement. In all cases, titania provided for high levels of improvement, while YSZ showed similarly high levels of improvements in some cases. Pure titanium coatings exhibited lower levels of improvement, indicating qualitatively that the lower wettability on metallic substrates (as compared to oxides) may play a role in dictating CHF improvements. Titanium, however, exhibits better adhesion to metallic substrates than do oxides, which is an important property for applications in a reactor environment. Given this, the improvements in CHF achieved by titanium coatings were sufficient to justify further study.

1.1. Introduction

Pool boiling on a heated surface can be described by a particular boiling regime with associated heat transfer coefficient. Nucleate boiling is defined by rapid vapor generation that produces many small bubbles and permits efficient heat transfer from the surface by latent heat transport and enhanced local convection. The critical heat flux (CHF) is the heat flux at which the boiling regime changes from nucleate boiling to film boiling, characterized by coherent vapor film blanketing of the heated surface. This transition results in heat transfer through the vapor layer that is orders of magnitude lower than that of nucleate boiling. Because of this sudden change, there is a sharp increase in surface temperature that can severely damage the heated surface.

At present, theories of CHF increase can be organized into four categories. These include theories of hydrodynamic instability, macrolayer dryout, hotspot/dryspot, and bubble interaction. The hydrodynamic instability theory was described as early as 1959 by Zuber [1] and later updated by Kutateladze [2] who arrived at the same equation form with a different leading constant. Subsequent theories built upon the latent heat removal mechanisms described in hydrodynamics but also expanded into other parameters such as wetting and dynamic contact angles. The macrolayer dryout theory was proposed by Haramura and Katto [3]. This model is primarily concerned with the regions of liquid formed underneath bubbles on the substrate surface. Current literature still cannot accurately describe the temperature gradient of this liquid layer. In 2006, Theofanous [4] proposed the hotspot/dryspot model using micro-hydrodynamics, which examines the meniscus of the fluid wetting the substrate surface near a bubble departure zone. CHF occurs as a runaway series of non-rewetting nucleation sites form on the heater surface. Kandlikar presented a theory reliant upon the liquid-to-vapor contact angle and the

contact angle with respect to the horizontal surface [5]. This model has since been modified to account for surface modification that can cause increased capillary wicking action and, thereby, produce a higher CHF [6].

Surface modification has been studied since the CHF was first shown to increase in water-based nanoparticle dispersions [7, 8]. Recent efforts have investigated coatings of nanoparticles on substrates without the use of nanofluid boiling [9]. In our related work, we have shown that surface coatings of nanoparticles can also be applied through a more reproducible electrophoretic deposition (EPD) technique [10]. These coatings demonstrate CHF enhancement trends that are similar to those produced by other techniques.

Our primary goal in this study is to determine the degree to which CHF could be enhanced through the use of EPD rather than nanofluid boiling, while also describing some of the underlying mechanisms for the observed increases. A thin wire was selected as the heater in order to draw comparisons with past CHF studies, many of which used a similar geometry [8, 9, 11]. EPD coatings were specifically examined because such coatings are mechanically robust compared to boiled-on coatings. This is advantageous for preventing chemical alteration of the coolant in a nuclear reactor, one potential application of this research. The application for Nuclear Engineering is that we started with a surrogate metal (stainless steel) and have progressed to a cladding material (zirconium). Finally, we are now testing actual cladding alloys (Zircaloy). These CHF enhancements have shown to be maintained and thus, we expect that as we transition to actual cladding tubular geometry, these CHF enhancements will be continued. This has direct application to improved heat transfer in actual cladding materials.

1.2. Experimental Procedure

1.2.1. Coatings

To establish an empirical comparison of these surface modification techniques, samples were pre-coated with nanoparticles via two methods, by boiling in a nanoparticle laden fluid and by the EPD technique. The former samples were held submerged in 500 ml of a rapidly boiling water-based nanofluid for 60 seconds. TiO₂ (7 nm average diameter) and ZrO₂ (20 nm) were used to prepare these nanofluids at 1% weight concentration in pure water. Coatings generated with this method were somewhat inconsistent in their uniformity and their thickness, likely due to an increasing nanoparticle concentration as the water gradually boiled away.

The samples coated via EPD were placed coaxially within a titanium tube in a vertical orientation. This tube was fixed within a pump-driven loop through which a nanofluid nominally at room temperature was circulated. The nanofluids utilized for EPD coatings were not water-based, but rather were prepared in an acetylacetone solvent with a minimal addition of triethanolamine (TEA) to aid in charging the particles. A constant voltage potential was applied between the titanium tube and the wire (the two electrodes) for between 5-10 seconds while pumping the solution at a nominal flow rate to provide a constant supply of suspended particles. The charged particles departed the solution to form the coating. Each solution that was prepared was used to coat six wires and the five best coated wires were used in CHF experiments. The configuration for EPD is depicted in Figure 1.

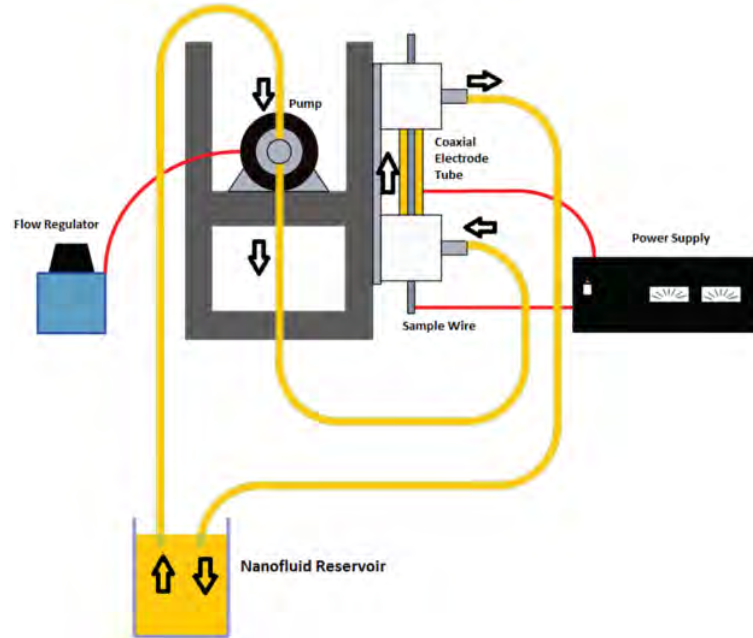


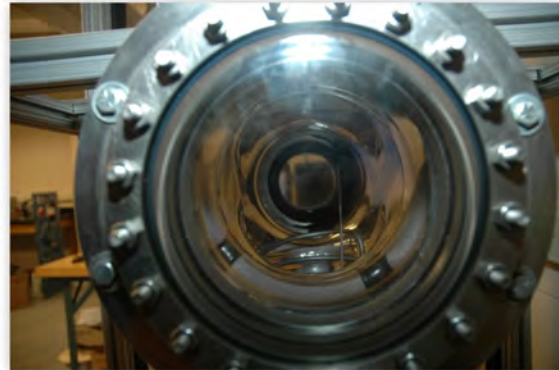
Figure 1: Schematic illustration of the EPD flow loop. A pump siphoned nanofluid from a reservoir, forcing it upwards through a titanium tube and past the wire sample, and then returning it to the beaker reservoir. Flow was maintained at 30 mL/s during the coating process.

1.2.2. Pool Boiling

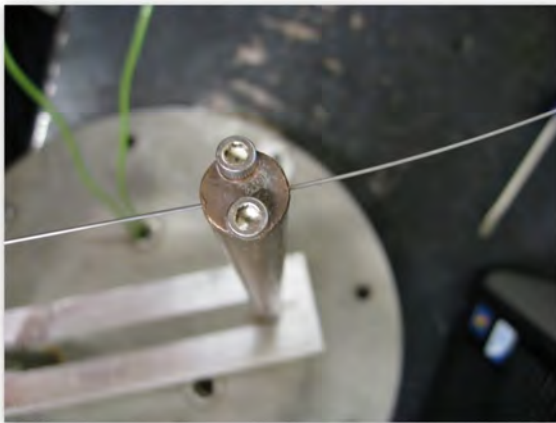
The pool boiling apparatus consisted of a 13.44 L cruciform tank of 0.5 inch thick Pyrex with an inner diameter of 6 inches. The tank was sealed on all ends with top and bottom plates featuring holes for thermocouples, a condenser, electrical hookups, and water egress (Figure 2a). The side plates featured viewports for observation of the boiling surface (Figure 2b). Two 14 inch long copper posts extended downwards from the top plate, holding wire samples in place in the center of the tank and conducting current to them (Figure 2c). A spring stretching between the top ends of the electrodes kept the sample under constant tension throughout the experiment, preventing deformation via thermal expansion (Figure 2d). A 20V-115A Sorenson power supply provided current which caused resistive heating in the sample. The wire samples used were 0.025 inch diameter wires of 316 stainless steel and 99.9% pure zirconium.



(a)



(b)



(c)



(d)

Figure 2: Hardware components of the pool boiling apparatus: (a) the Pyrex tank with condenser attached on top and coil heater in the bottom, (b) the sealing plates with windows at the horizontal ends of the tank, (c) end-on view of the copper electrodes which hold the wire, and (d) the top of the electrodes with a spring in between to keep the wire under tension during testing.

All bare samples were cleaned with ethanol and 1200 grit silicon-carbide paper prior to pool boiling experiments. EPD-coated samples were cleaned prior to coating. The sample heaters were positioned with a length of approximately 3.33-3.34 inches. Voltage leads attached to the ends of the wire measured the voltage drop across the heated length. This, coupled with a Hall Effect probe current measurement, was used to determine the thermal power output of the wire.

The heat flux on heated wire is determined by total power from output current and voltage of the power supply and the surface area of the wire using the expression: $q'' = \frac{V \cdot I}{A} = \frac{V \cdot I}{\pi \cdot D \cdot L}$

A schematic of this arrangement is depicted in Figure 3.

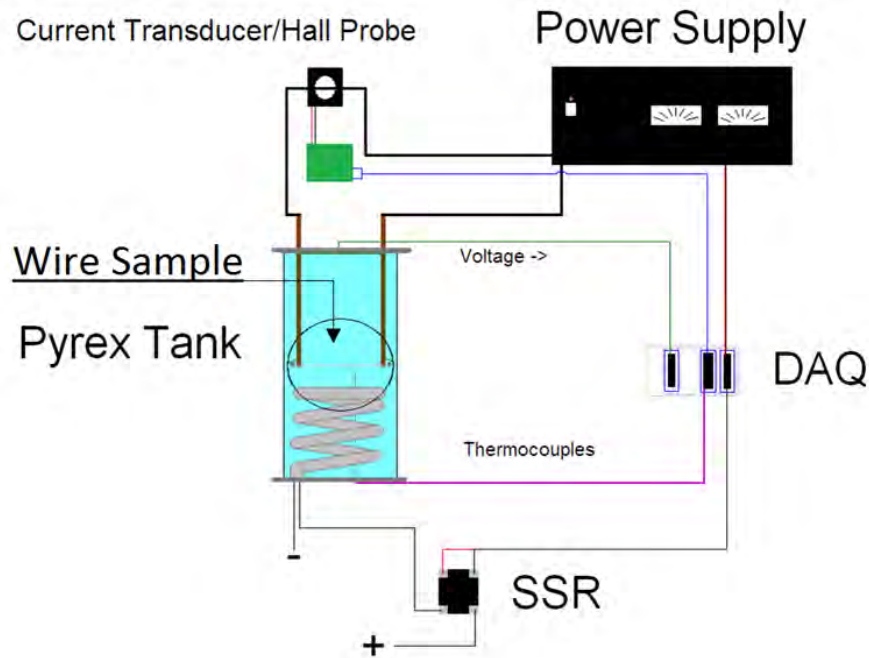


Figure 3: Schematic illustration of pool boiling CHF test apparatus. The wire sample was placed between two copper posts inserted into a 13.4 L Pyrex tank.

The sample wire, being in-circuit with the power supply via the copper electrodes, was first submerged in water or nanofluid within the Pyrex tank. A large coil heater in place at the bottom of the tank heated the liquid medium to saturation and then boiled it for an additional 10 minutes. Throughout this process, a low-level voltage of approximately 0.2 V was applied across the wire to document the change in resistance as the wire was heated. After 10 minutes of boiling the heater was shut off and, after bubble generation stopped, the voltage across the wire was gradually ramped up. A LabVIEW control automated this ramp so as to increase the power

output linearly. The increment of power ramp is 0.2W. The test concluded when there was a departure from nucleate boiling (DNB) after which the wire developed a hot spot and broke.

Table 1: Experimental parameters and coating conditions investigated in the present study. Variables were particle size, metal-oxide species, and coating method. Titanium coatings were also tested. “Nanofluid Medium” coatings were applied in-situ during pool-boiling CHF experiments. EPD coatings were applied in advance by EPD process. Boiled-on coatings were applied in advance by submerging the heater samples in boiling nanofluid.

		7 nm	15 nm	20 nm	20-30 nm	40-80 nm	45 nm	50 nm	50 nm (hydrophilic)	60-80 nm	250 nm
TiO ₂ :	Nanofluid Medium	SS	SS, Zr					SS, Zr	SS		SS
	EPD Coating	SS						Zr	SS	Zr	SS, Zr
	Boiled-on Coating	SS									
Al ₂ O ₃ :	Nanofluid Medium		SS			SS, Zr					
	EPD Coating		SS								
ZrO ₂ :	Nanofluid Medium			SS			SS				
	EPD Coating			SS							
	Boiled-on Coating			SS							
YSZ:	Nanofluid Medium				SS, Zr						
	EPD Coating				SS, Zr						
Titanium	EPD Coating									Zr	

Pool boiling tests were conducted on coated and uncoated samples in high-purity distilled water (18.2 MΩ-cm) and in nanofluids prepared with this water. Nanofluids and coatings utilized nanoparticles of four single-metal oxides (titania, zirconia, yttria-stabilized zirconia, and alumina) with a variety of particle sizes and concentrations. Titanium metal coatings were also tested due to superior adhesion compared to oxides. First, 7 nm titania nanofluids were tested at concentrations of 0.1%, 0.05%, 0.01%, 0.005%, and 0.001% by weight. This set of tests determined that 0.005% was an ideal concentration for CHF enhancement. Therefore, all subsequent nanofluid-medium tests were conducted at 0.005% concentration by weight in water.

Table 1 (above) summarizes the various nanofluids and coatings investigated in the present study. Additionally, clean wires were tested in clean water to establish a baseline value for CHF with stainless steel and zirconium wires.

1.3. Experimental Results

1.3.1. Boiling curves Zirconium wires

Figure 4 indicates boiling curves of bare wire in pure water, YSZ 20-30nm 0.005% containing nanofluid boiling, and YSZ EPD coated wire boiling experiments for zirconium wire material. The surface temperature of the wire was evaluated using the temperature coefficient using the resistance method. As may be noted, the EPD and nanofluid boiling curves are very similar, and their heat transfer coefficients are lower than that of the bare wire in pure water.

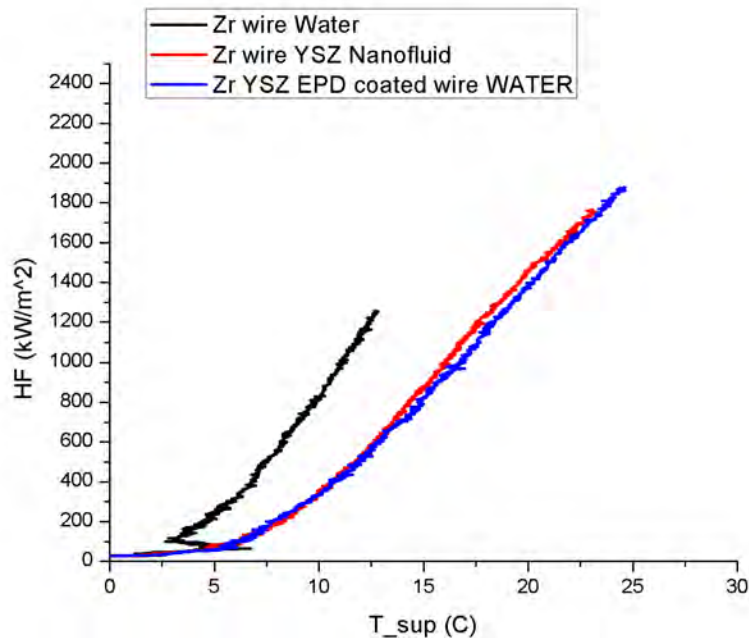


Figure 4: Boiling curves for 0.625mm Zirconium bare wire in pure water, wire 20-30nm YSZ coated using EPD in pure water, and bare wire in 20-30nm YSZ 0.005wt% nanofluid.

1.3.2. CHF of Stainless Steel and Zirconium in Water

The baseline CHF value determined by testing uncoated stainless steel wires in high purity distilled water was 1147 kW/m² (Figure 5). The error bar for experimental data in Figures 5 - 7 represents the uncertainty of 2.4% on the heat flux resulting from the combined effects of current, voltage, heated length, and wire diameter. Tests of clean samples in pure water were done first to prevent any contamination effects in the apparatus from subsequent nanofluid runs. This sensitivity to even miniscule concentrations of nanoparticles is shown in Figure 6, where small amounts of nanoparticle deposits were observed even after cleaning the system. Due to this influence, the apparatus was regularly disassembled and cleansed after experiments involving nanoparticles. This yielded results consistent with the tests in clean water.

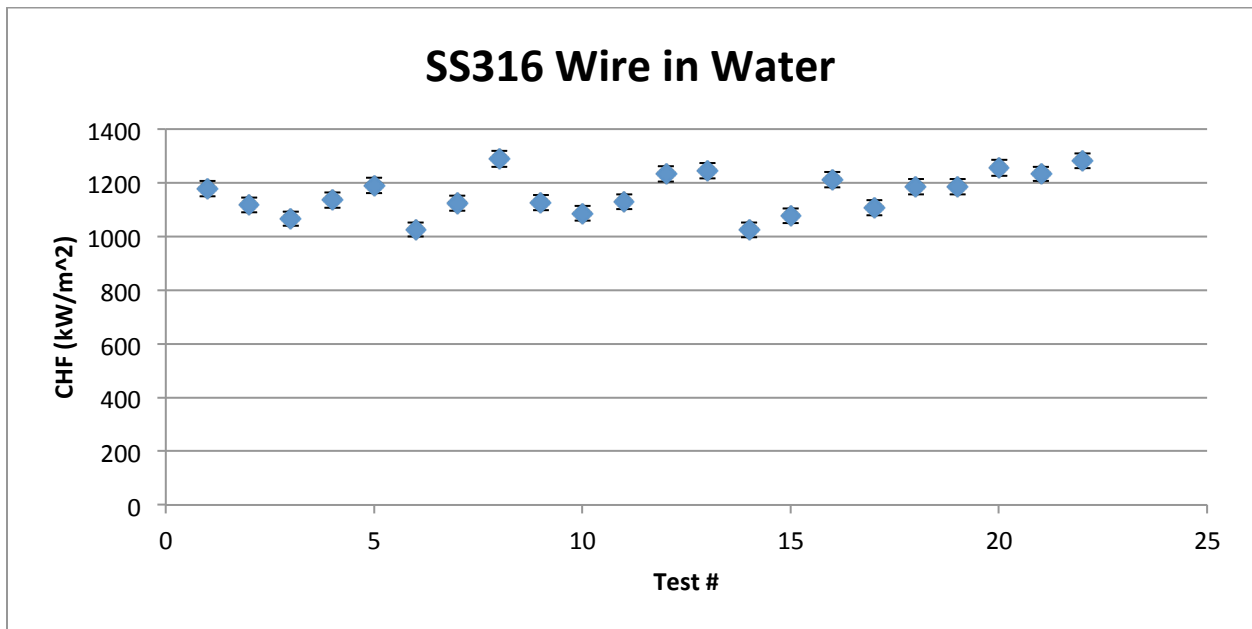


Figure 5: The critical heat flux values of 316 stainless steel wires measured in high purity distilled water.

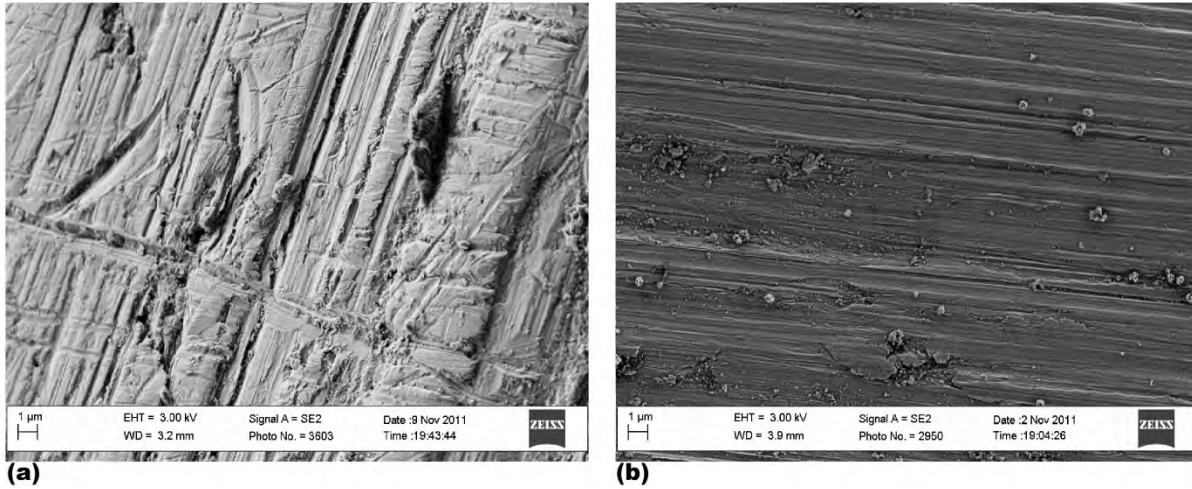


Figure 6: A demonstration of the need to thoroughly clean the system after CHF experiments involving nanofluids (a) SEM image of bare stainless steel substrate after CHF testing in clean water in an unused tank. (b) SEM image of the bare stainless steel wire in clean water after nanofluid runs had been conducted. The CHF values are 1185 and 1362 kW/m², respectively. Average CHF for clean stainless steel samples in clean water after thorough cleanings remained within +/- 10% of the 1147 kW/m² baseline.

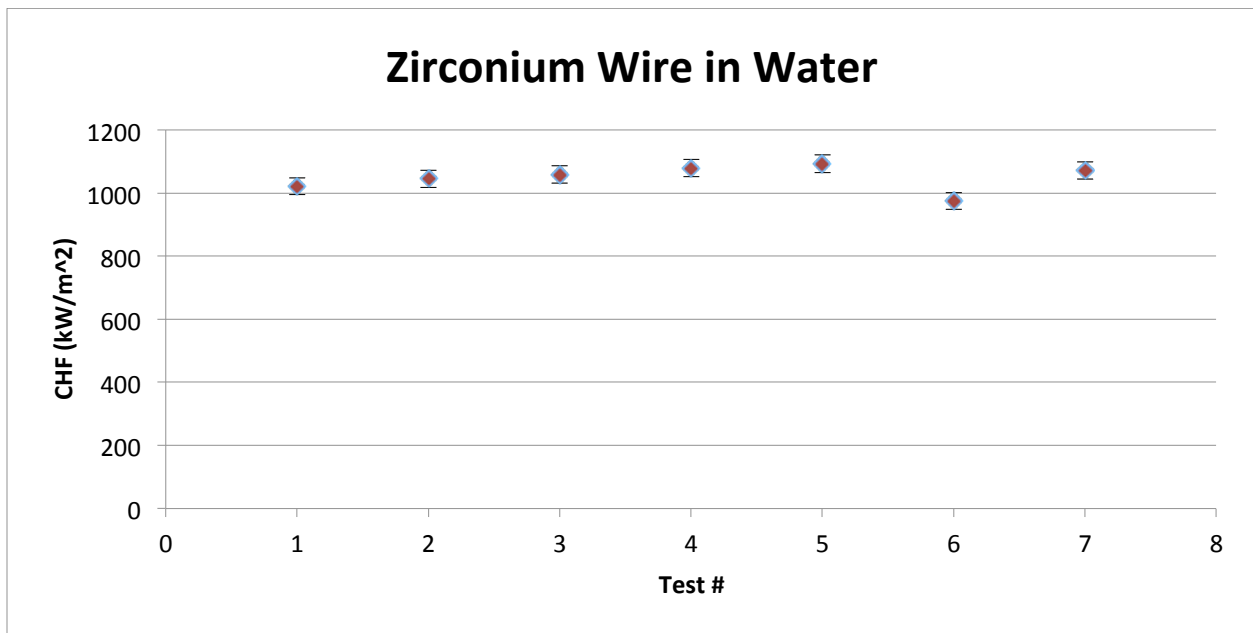


Figure 7: The critical heat flux values of zirconium wires measured in high purity distilled water.

The baseline CHF values for zirconium wires in clean water was determined to be 1034 kW/m² (Figure 7). Subsequent data demonstrate a consistent trend of lower CHF for zirconium

wire under the same conditions as stainless steel wire tests. Surface roughness did not play a role in this observed difference between the two materials given that samples were prepared identically for all experiments. For this reason, Zuber [1] and Kutateladze [2] models that do not include material properties may not be adequate for a complete description of CHF.

1.3.3. CHF of Bare Stainless Steel and Zirconium in Nanofluid

The samples boiled in a nanofluid solution experienced a range of CHF enhancements depending upon the species and size of the nanoparticles. 7 nm TiO₂ was tested at a variety of concentrations; this did not have an apparent effect upon the CHF value above concentrations of 0.001 wt.%, consistent with the work by Kim [12, 13]. Figure 8 shows the CHF results of the five different titania concentrations. Scanning electron microscope (SEM) images of the wire surfaces were taken for a selection of the tests (Figure 9). Wires tested in nanofluids showed significant enhancement in the CHF value compared to those tested in clean water (Figure 10). The level of CHF enhancement was independent of particle size and nanoparticle species. However, there was less deviation in titania nanofluids for which there was also a trend towards more deviation with larger particle size. After determining optimal concentration conditions, various sizes of titania were tested in nanofluid on the stainless steel wires. Agglomeration effects are seen for the 15 nm titania, but decreased in size with increasing particle size, as shown in Figure 11. Agglomerations are on the scale of microns, and in many cases agglomerates as large as 10 microns were observed for the 15 nm particles. Despite these cluster formations, larger particle sizes with more uniform surface characteristics trend with lower CHF values than do wires coated in smaller particles.

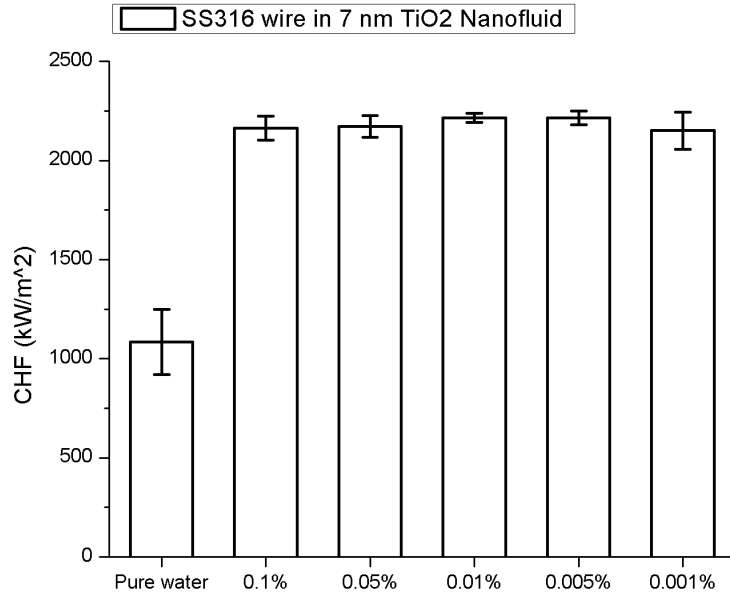


Figure 8: The critical heat flux values for 316 stainless steel wires tested in nanofluids containing various concentrations of TiO₂ nanoparticles.

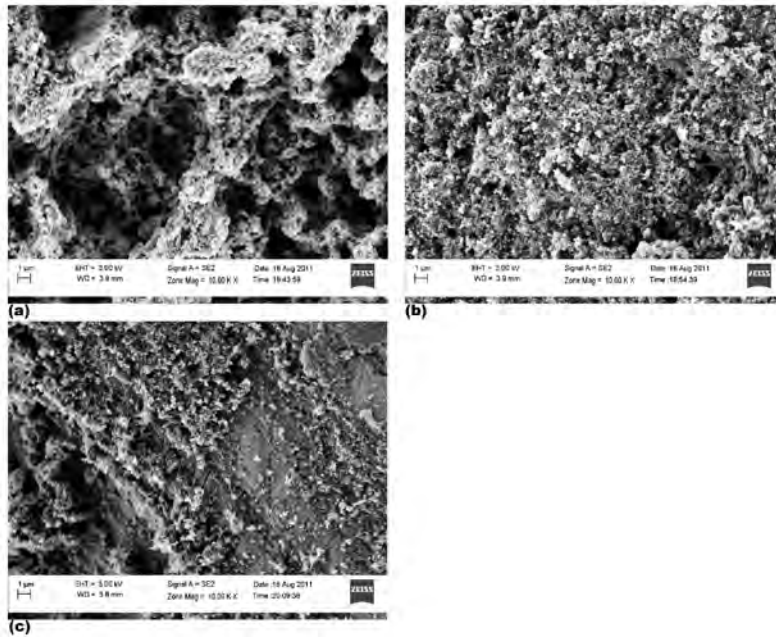


Figure 9: SEM images of uncoated stainless steel 316 sample heaters after burnout during CHF experiments conducted in nanofluids containing 7 nm TiO₂ nanoparticles of the following concentrations: (a) 0.05%, (b) 0.01%, and (c) 0.005%. EDS results confirmed the deposited structures were composed of TiO₂. Despite different deposit morphologies, the CHF values of all three samples were within 5% of 2200 kw/m².

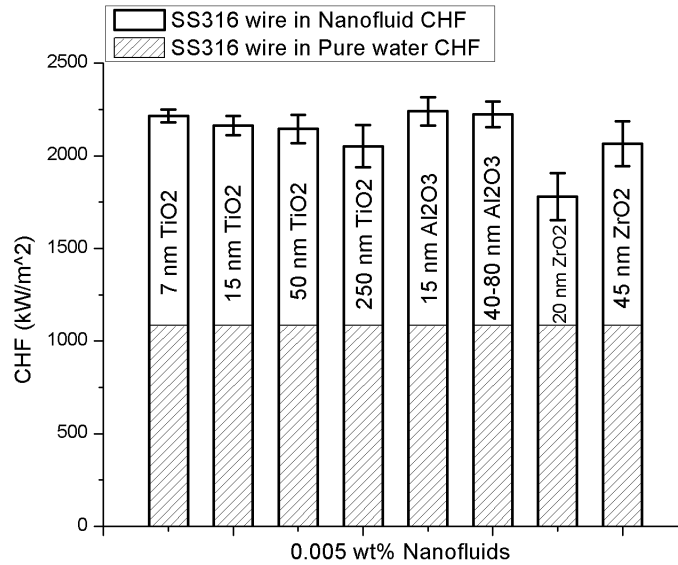


Figure 10: Critical heat flux values for 316 stainless steel wires tested in a variety of nanofluids with various nanoparticle sizes and species.

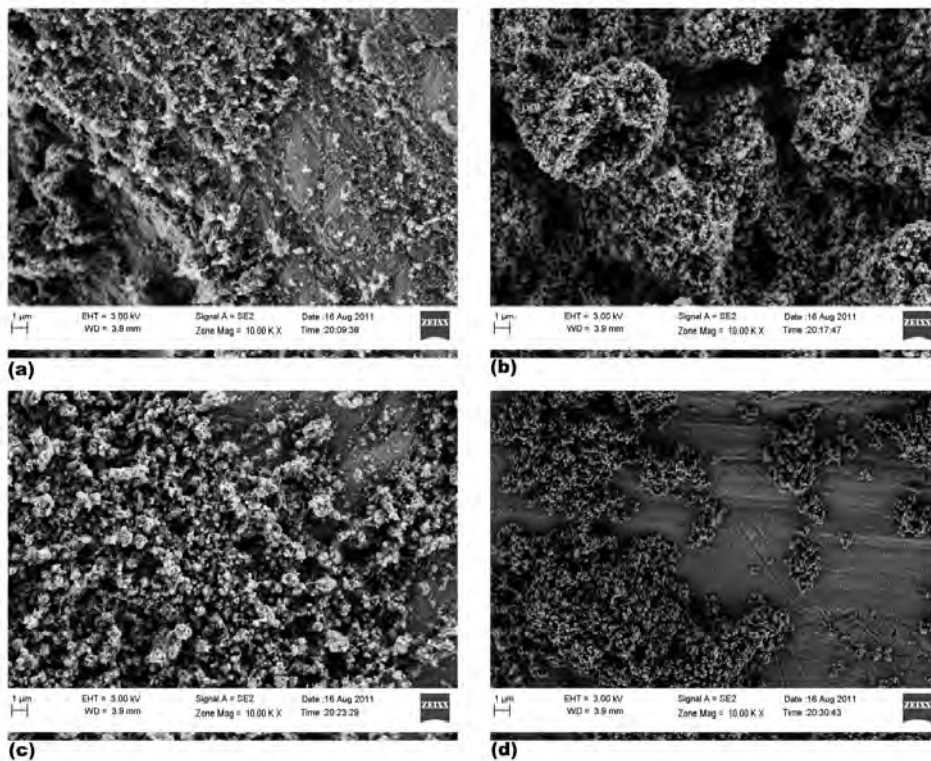


Figure 11: SEM images of bare 316 stainless steel wire surfaces after CHF experiments performed in nanofluids containing nanoparticles of TiO₂ of various sizes: (a) 7 nm, (b) 15 nm, (c) 50 nm, and (d) 250 nm.

However, as will be shown later, this particle-size trend diminishes in the wire samples EPD-coated with titania. A reason for this may be a lack of coating coverage on the surface during nanofluid boiling. Further data exhibit lower CHF on samples with minimal coatings when compared to fully-coated substrates. Larger particles may fall out of suspension during nanofluid boiling and prevent adequate surface coating. Therefore, a trend towards lower CHF enhancement using larger particles in solution may be due to coating mechanisms rather than differing coating interactions within the pool boiling environment.

Table 2 summarizes the CHF enhancements for various experimental conditions used with bare stainless steel and zirconium wires with regards to nanofluid tests. It can be noted that CHF tended to decrease with increasing particle size. As this pattern was not evident in EPD pre-coated wires, sedimentation was likely driving this decrease in CHF values. Oxide densities are 4.23, 3.95-4.1, and 5.68 g/cm³ for titania, alumina, and zirconia, respectively. For a single particle size, the denser species used in a nanofluid produced the lesser CHF enhancement, which further supports the role of sedimentation.

Table 2: A listing of the CHF results and standard deviations for nanofluid experiments on 316 stainless steel wires.

Nanoparticle Species and Size	Average CHF Value (kW/m ²)	Average CHF Enhancement (compared with water)	CHF Standard Deviation (kW/m ²)
7 nm Titania	2211.75	1.93	37.85
15 nm Titania	2145.50	1.87	36.92
50 nm Titania	2116.25	1.85	47.08
250 nm Titania	2013.42	1.76	86.47
15 nm Alumina	2235.75	1.95	83.80
40-80 nm Alumina	2205.83	1.92	57.74
20 nm Zirconia	1731.58	1.51	84.79
45 nm Zirconia	2015.58	1.76	69.62
20-30 nm YSZ	1829.62	1.60	195.50

Fewer nanoparticle studies were conducted for zirconium wires than for stainless steel wires. The primary goal of the nanofluid zirconium tests was to confirm enhancement akin to that observed with stainless steel. Zirconium nanofluid data is shown in Figure 12.

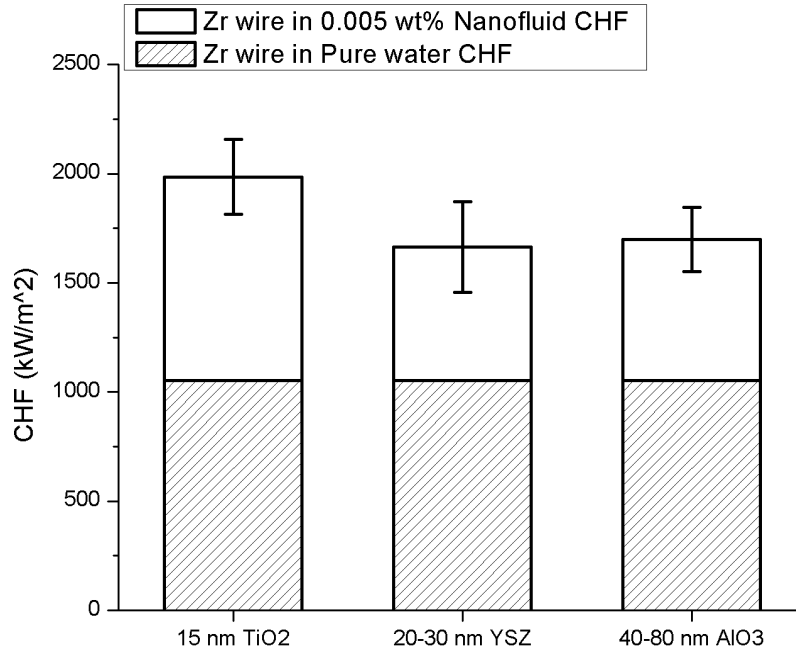


Figure 12: Critical heat flux values for zirconium wires tested in a variety of nanofluids with various nanoparticle sizes and species.

Titania resulted in the highest levels of improvements with a CHF value of 2211.75 kW/m².

Standard deviations are larger among zirconium tests than the stainless steel tests (Table 2 and 3).

Table 3: A listing of the CHF results and standard deviations for nanofluid experiments on zirconium wires.

Nanoparticle Species and Size	Average CHF Value (kW/m ²)	Average CHF Enhancement (compared with water)	CHF Standard Deviation (kW/m ²)
15 nm Titania	2043.66	1.98	84.65
20-30 nm YSZ	1732.14	1.67	158.0
40-80 nm Alumina	1632.43	1.72	144.7

CHF enhancements by nanofluid on the bare wires and in pure water on the EPD coated wires are very similar as we have shown in Tables 2, 3, 4, and 5 of the manuscript. Moreover, the boiling curves also have strong similarities. Therefore, we have speculated with a high degree of certainty that nanoparticle surface coating is the main factor of pool boiling CHF enhancement.

Table 4: A listing of the CHF results and standard deviations for EPD-coated SS316 wire experiments.

Nanoparticle Species and Size	Average CHF Value (kW/m ²)	Average CHF Enhancement (compared with water)	CHF Standard Deviation (kW/m ²)	% of Nanofluid Enhancement
7 nm Titania	1968.82	1.72	157.56	89
20 nm Zirconia	1713.25	1.49	97.69	99
15 nm Alumina	1805.67	1.57	49.74	81
20-30 nm YSZ	2160.94	1.88	102.32	120

Table 5: A listing of the CHF results and standard deviations for EPD-coated zirconium wire experiments.

Nanoparticle Species and Size	Average CHF Value (kW/m ²)	Average CHF Enhancement (compared with water)	CHF Standard Deviation (kW/m ²)
20-30 nm YSZ	1766.07	1.71	137.1
50 nm rutile titania	1717.47	1.74	207.1
60-80 nm Ti	1435.879795	1.39	107.4

In support of our findings and conclusions, Kim et al [8] have demonstrated that transport and thermodynamic properties of dilute nanofluid were very similar to those of pure water by measurement of the surface tension, thermal conductivity and viscosity of nanofluids.

1.3.4. CHF of EPD-Coated Stainless Steel and Zirconium in Water

EPD coatings of 7 nm TiO₂, 20 nm ZrO₂, 15 nm Al₂O₃, and 20-30 nm YSZ were applied to clean stainless steel wires. These wires were identical to those previously used during CHF

experiments in both clean water and nanofluids. Estimated of TiO₂ EPD coating thickness on Zr wire was obtained from SEM images. The thickness is of the order of 4 μm to 6 μm, so the coating thicknesses are typically only about 1% of the wire diameter (Figure 13).

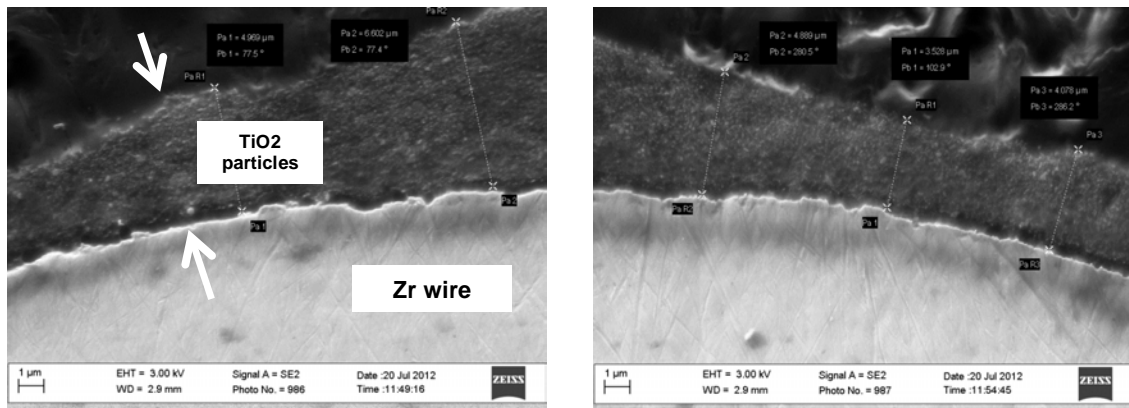


Figure 13: SEM images showing thickness of 60-80nm titania EPD coating on bare Zirconium wire. The light gray portion is the Zirconium wire, whereas the darker surrounding indicates titania particles.

Titania and YSZ coatings demonstrated, on average, larger CHF enhancement than either zirconia or alumina (Figure 14). 20-30 nm YSZ, 50 nm titania, and 60-80 nm titanium particles were deposited on zirconium wire by the EPD technique. In this case the two oxide coatings, YSZ and titania, exhibited higher CHF enhancement than pure titanium metal (Figure 15). The results of CHF studies on EPD coated stainless steel and zirconium wires are summarized in Tables 4 and 5.

Titanium particles were tested due to their improved adhesion to zirconium substrate, whereas most oxide coatings are more susceptible to flaking. 250 nm titania was also studied due to its stronger adhesion as compared to EPD coatings of smaller particles of the same material. Coatings were more robust and resilient to cracking (as observed by optical microscope images) for nanoparticles of 250 nm size. SEM images of flat samples coated with titania demonstrated

that smaller particles agglomerated together in scattered areas. These sites of agglomeration caused tensile stress on the surrounding particles and thus initiated surface cracking. A comparison of these coatings is shown in Figure 16. All coatings were deposited for the same amount of time and using the same EPD conditions. Titanium coatings exhibit a much lower CHF increase than oxide coatings on either substrate. This would suggest that there may be wetting effects involved in CHF [5, 8], as oxides wet much better than metallic substrates.

Figure 17 demonstrates the differences between nanofluid boiling and EPD coating experiments. An EPD-coated zirconium sample is shown before experimentation and again after CHF. The post-CHF image exhibits the change in coating morphology during the experiment. The coating becomes less uniform and begins to adopt a coral-like structure. This structure is similar to that shown in Figure 16b with fewer sites of agglomeration. The final image of the series is taken after CHF in a nanofluid boiling experiment. The coating is much thinner than the EPD-coated sample after CHF. Additionally, the CHF determined for this sample is lower than that of the EPD sample. This suggests that a more uniform coating is more beneficial than scattered agglomerations on the substrate. This is reinforced by the titanium EPD-coated samples shown in Figure 18. Values of CHF for titanium coated zirconium wires are shown in Figure 19.

Sparse coatings of 60-80 nm metallic titanium on zirconium wires showed less CHF enhancement than wires with greater coverage. This supports the idea of variation among the titania nanofluid pool boiling data due to differences in coverage rather than particle size. CHF data for the titanium EPD coatings are also shown below. Though metallic coatings have produced less CHF enhancement than oxide coatings, they are favorable with regards to improved substrate adhesion.

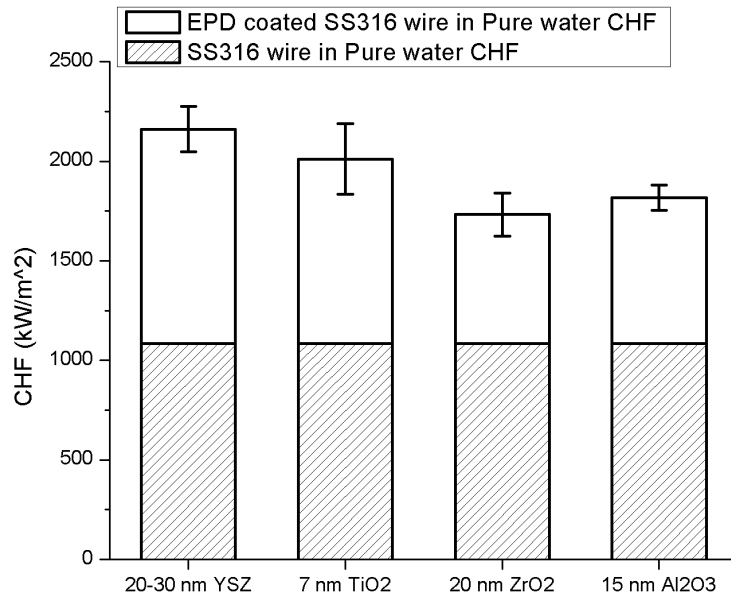


Figure 14: Critical heat flux values for stainless steel wires coated with nanoparticles of various sizes and species and tested in water.

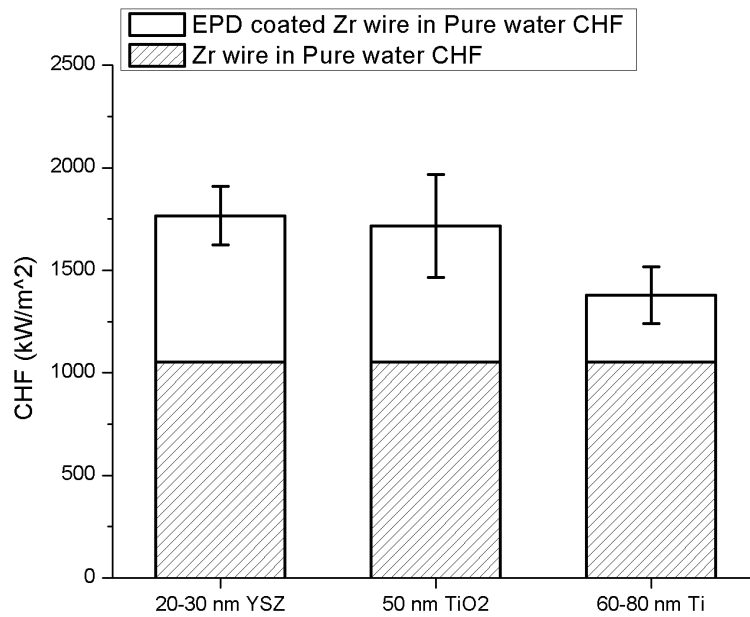


Figure 15: Critical heat flux values for zirconium wires coated with nanoparticles of various sizes and species and tested in water.

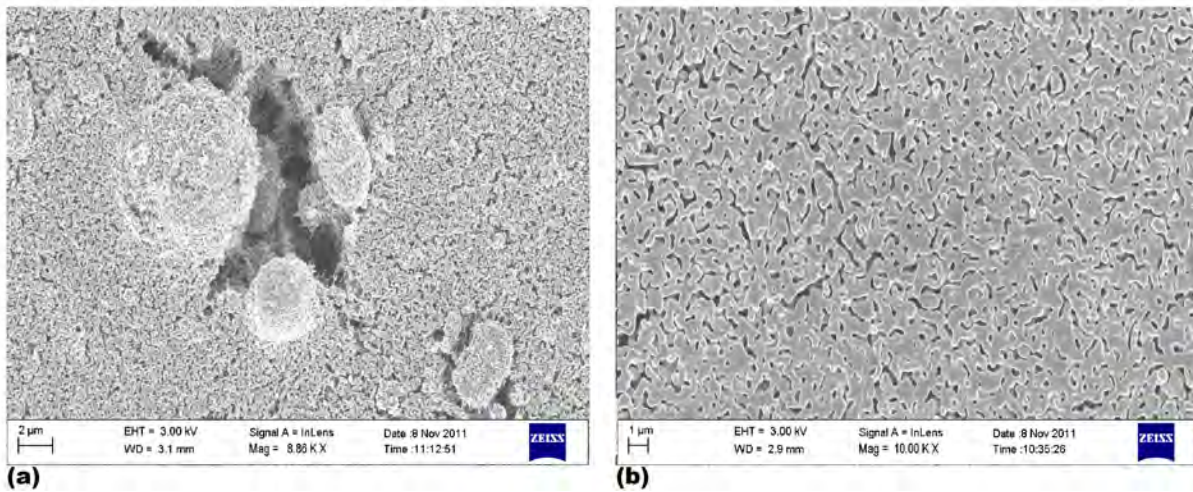


Figure 16: (a) SEM images of 30-50 nm TiO₂ at 8.86kx magnification and (b) 250 nm rutile TiO₂ at 10kx magnification. Cracking forms around large agglomerations of particles in the 20-30 nm species. Coatings of 250 nm TiO₂ present no cracks and are visibly homogenous in structure.

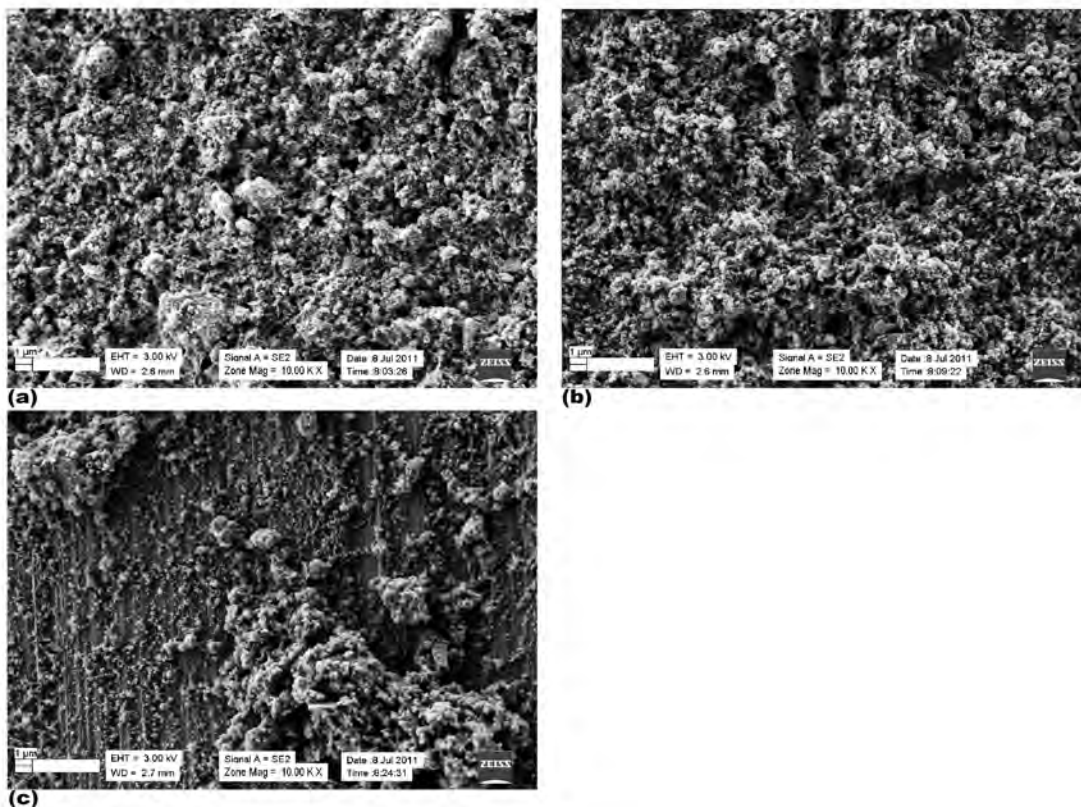


Figure 17: (a) Zirconium wire samples with 20-30 nm YSZ nanoparticles are shown as deposited after EPD, (b) after EPD and boiling CHF, and (c) as deposited during a nanofluid boiling CHF experiment. The CHF values of the EPD and nanofluid sample are 1996 and 1729 kW/m², respectively.

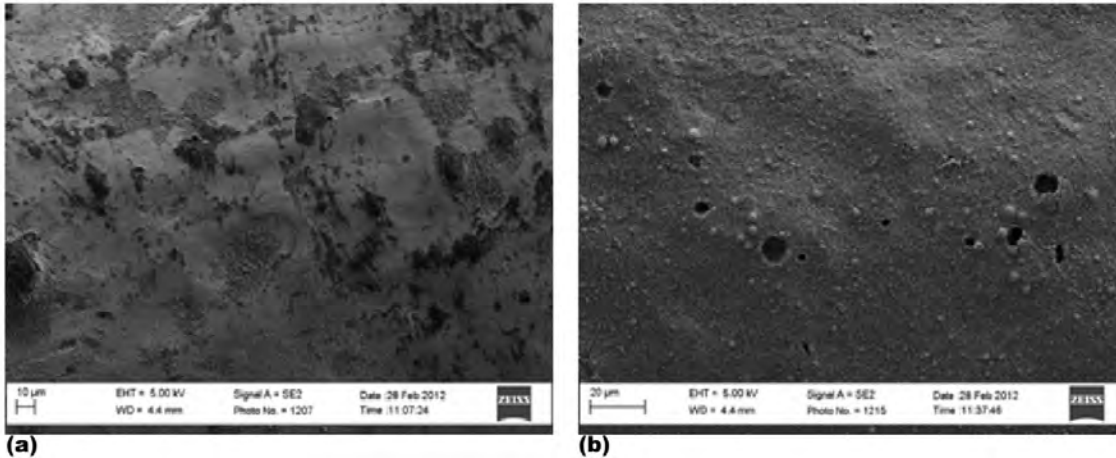


Figure 18: SEM images of metallic titanium EPD-coated zirconium wire after CHF test. Both wires were coated under the same conditions. Due to some variability in final coating, the samples reached (a) 1262 and (b) 1510 kW/m² during CHF testing. The coating on (a) is incidentally sparse and is likely the reason for lower enhancement.

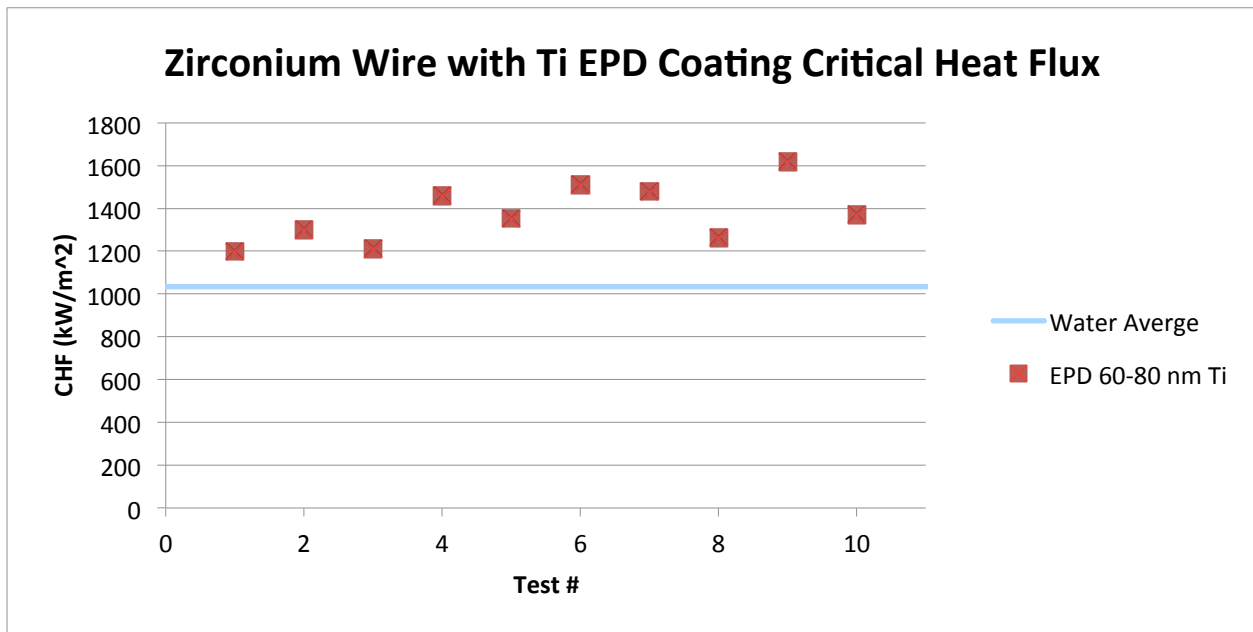


Figure 19: Critical heat flux values for EPD coatings of 60-80 nm metallic titanium on zirconium wire. Titanium provides a lower enhancement than oxide coatings, with an average of 40% CHF increase.

Figure 18 also demonstrates a microstructure that was not observed in the oxide samples after burnout. Titanium EPD samples on zirconium exhibit craters varying between 3 and 20

microns in diameter among the samples that had high CHF enhancement. These sites are suspected to be bubble departure locations prior to burnout. Visualization experiments conducted by Nishio [14] demonstrate increasing vapor departure size with increased heat flux of the sample heater. Because of these large assumed departure sites, larger vapor bubbles could be released from the surface compared to the samples with sparse coatings.

Figure 20 below shows additional SEM images of a sample with low CHF enhancement. Unlike the sample shown in 18a, this sample is fully coated. However, it features smaller crater regions than those evident in higher-CHF samples. If these are bubble departure sites, they represent diameters 1000 times smaller than those found in water CHF images [14]. This has significant implications for CHF correlations pertaining to bubble departure diameter. Despite the evidence of smaller diameter bubbles, titanium-coated substrates still have a higher CHF than bare substrate in water.

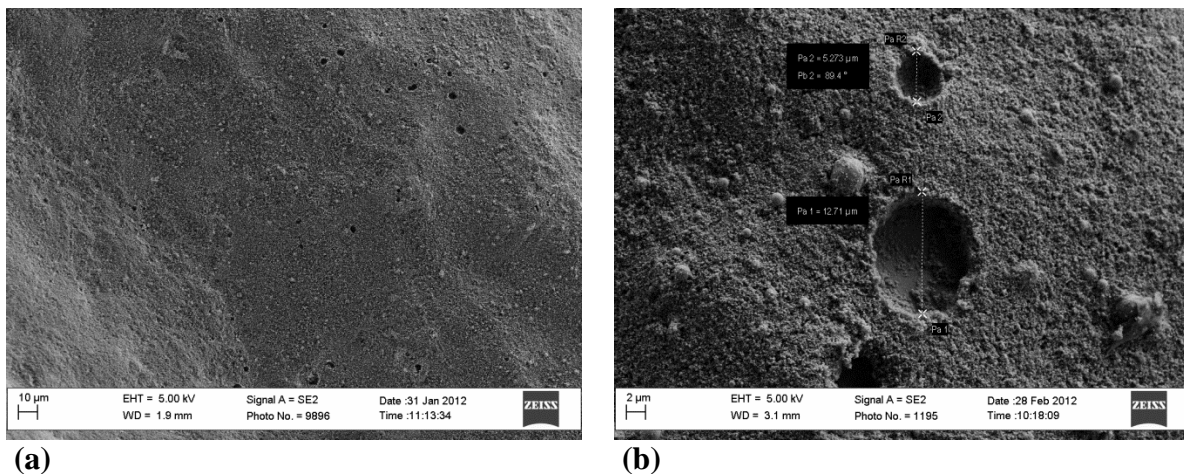


Figure 20: Titanium EPD coated zirconium wire after burnout. The top image (a) is taken at 1kx magnification and show few crater regions. Further examination of these sites (b) shows the sizes of these features are 2-5 times smaller than those found in the samples with high CHF. However, both samples exhibit smaller craters. It is suspected that these areas are formed after vapor build-up is released from the underlying substrate.

1.3.5. CHF of Boiling-Coated Stainless Steel Samples in Water

To mimic past demonstrations of coating-induced CHF enhancement, wires were coated separately in boiling water containing 7 nm TiO₂ and 20 nm ZrO₂ (i.e. the boiling method) and then tested for CHF in clean water. CHF data for these experiments is shown in Table 6. The average CHF value reached with these coatings was within one standard deviation of that obtained with EPD coatings. Figures 21 and 22 compare CHF values for each method of coating for 7 nm TiO₂ and 20 nm ZrO₂. These values are within experimental error of EPD sample experiments on stainless steel.

Table 6: A listing of the CHF results and standard deviations for boiling-coated wire experiments.

Nanoparticle Species and Size	Average CHF Value (kW/m ²)	Average CHF Enhancement (compared with water)	CHF Standard Deviation (kW/m ²)
7 nm Titania	2060.50	1.80	63.00
20 nm Zirconia	1763.67	1.54	88.11

The data and images show that there is particle deposition on the substrate during nanofluid pre-boiling that is comparable to EPD. It would be expected that the coatings produced by the boiling approach would produce the same CHF enhancement as in nanofluid tests. In order to check it statistically, test of hypothesis with Bonferroni Correction have been conducted to make comparisons between experiments using EPD coated wires in pure water, nanofluid boiling coated wires, and bare wires in pure water. The level of significance is 0.05. According to these statistical tests, there exists a statistically significant increase in CHF using either nanofluids or EPD coated wires compared to bare wires in pure water. There, however, is not sufficient evidence to say that EPD coatings and nanofluid boiling coatings have significant difference. The average CHF enhancement in nanofluid tests is, however, significantly larger

than that of pre-boiled samples. This may indicate that particles are removed from the surface during nucleate boiling.

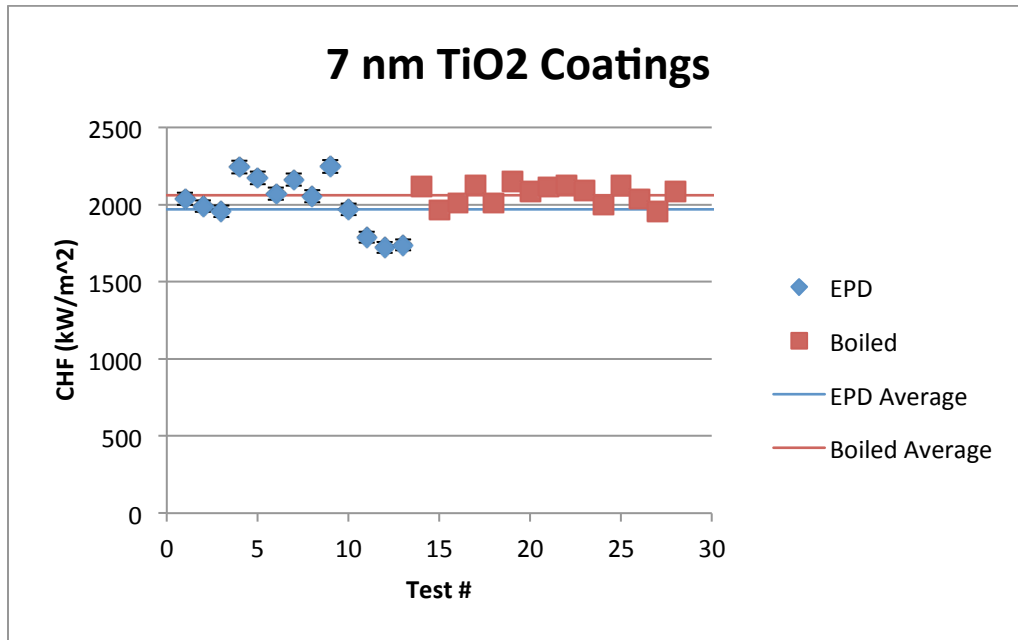


Figure 21: A comparison of CHF values observed on wires coated with 7 nm titania particles via EPD and boiling methods.

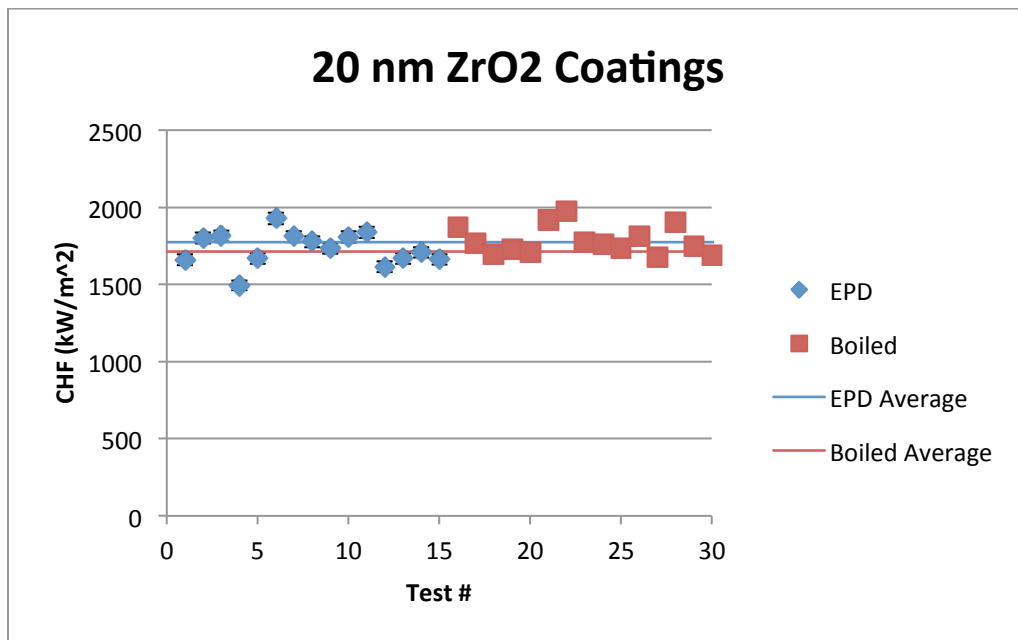


Figure 22: A comparison of CHF values observed on wires coated with 20 nm zirconia particles via EPD and boiling methods.

1.4. Conclusion

Enhancement of Critical Heat Flux would be a significant step towards providing for more accident-tolerant conditions in a nuclear reactor. An experimental system to determine CHF in a pool-boiling environment using wire-configuration samples with nanoparticle surface modification heated by electrical resistive heating was designed and constructed. The electrical power supplied to the wire was gradually ramped until the point at which the boiling regime changes from nucleate boiling resulting in hot spots on the wire, in turn resulting in its instantaneous rupture.

Using this experimental facility it has been shown that dispersion of oxide nanoparticles in water (nanofluid) in concentrations as low as 0.005% or deposition of nanoparticle -based coatings on the wires can result in significant enhancement of CHF. For the nanofluid study, titania, zirconia, yttria-stabilized zirconia and alumina nanoparticles of various sizes and concentrations were studied. It was determined that a concentration of 0.005% yielded reproducible improvements in CHF. In the regime of particle sizes studied, all particle sizes resulted in similar improvements in CHF, but at larger sizes a slight drop in CHF was observed possibly due to sedimentation effects. Since larger particles are more readily affected by gravity and fluid flow, they tend to 'sink' rather than stick to wire surface. Furthermore, those that do stick to the wires are more likely to get detached on the surface during subsequent boiling. Finally, larger size particles tend not to be dispersed uniformly in the fluid. Zirconia resulted in slightly lower improvements than YSZ, titania and alumina. Coating the wires with the nanoparticle layers by electrophoretic deposition (EPD) with titania and alumina resulted in higher CHF enhancement than with zirconia. These experiments suggest that CHF enhancements for tests performed in nanofluids result from an in situ formation of a nanoparticle layer on the

wire sample surface. Between the two processes examined, the deposition of coatings on wires by the EPD coating technique (rather than altering the composition of the water coolant) is likely to be a more commercially attractive option.

It is hoped that further testing will demonstrate the viability of applying coatings to thicker cylindrical rods using the coaxial flow deposition process investigated in this study and that these rods can then be tested for CHF enhancement. Other needed work includes further examination of metallic EPD coatings to resolve issues of lower enhancement when compared to oxide coatings and to establish the role of surface wetting effects.

Finally, our approaches to mechanism of CHF enhancement are summarized as follows:

- Past hypotheses by other investigators have suggested contact angle effects from the transient and steady-state wetting behavior, but that is not verifiable by measurements connected to boiling.
- We have photographs and videos of the boiling process on these wires but we expect the real mechanistic effects are not directly observable.
- We are now trying to use our ability to take hi-speed video measurements of the boiling behavior and breakdown the behavior into active nucleation sites, bubble departure frequency and bubble departure sizes as a function of the operating heat flux and the surface modification by nanoparticles.
- We anticipate these more detailed measurements will help us isolate what boiling parameters are affected by the surface modifications and hope to link it to surface materials effects.

1.5 References

- [1] N. Zuber, Hydrodynamic Aspects of Boiling Heat Transfer, AECU-4439, 1959.
- [2] S.S. Kutateladze, A hydrodynamic theory of changes in a boiling process under free convection, in: *Izvestia Akademia Nauk, S.S.S.R., Otdelenie Tekhnicheskii Nauk*, vol. 4, 1951, p. 529.
- [3] Y. Haramura, Y. Katto, A new hydrodynamic model of critical heat-flux, applicable widely to both pool and forced-convection boiling on submerged bodies in saturated liquids, *Int. J. Heat Mass Transfer* 26 (3) (1983) 389–399.
- [4] T.G. Theofanous, T.N. Dinh, High heat flux boiling and burnout as microphysical phenomena: mounting evidence and opportunities, *Multiphase Sci. Technol.* 18 (1) (2006) 1–26.
- [5] S.G. Kandlikar, A theoretical model to predict pool boiling CHF incorporating effects of contact angle and orientation. In: *Heat Transfer* 123 (2001) 1071-1079
- [6] H. Ahn, C. Lee. The Effect of capillary wicking action of micro/nano structures on pool boiling critical heat flux. In: *International Journal of Heat and Mass Transfer* 55 (2012) 89-92
- [7] S. Choi, Enhancing thermal conductivity of fluids with nanoparticles in: D.A. Siginer, H.P. Wang (Eds.), *Developments and Applications of Non-Newtonian Flows*, ASME, FED-231/MD-66, 1995, pp. 99-105
- [8] S.J. Kim, I.C. Bang et al. Surface wettability change during pool boiling of nanofluids and its effect on critical heat flux. In: *International Journal of Heat and Mass Transfer* 50 (2007) 4105-4116

- [9] E. Forrest, E. Williamson et al. Augmentation of nucleate boiling and critical heat flux using nanoparticle thin-film coatings. In: International Journal of Heat and Mass Transfer 53 (2007) 58-67
- [10] Lucas Wilson, Development of Diffusion Barrier Coatings for Mitigation of Fuel-Cladding Chemical Interactions, MS Thesis Nuclear Engineering and Engineering Physics, University of Wisconsin – Madison
- [11] B. Stutz, C. Morceli et al. Influence of nanoparticle surface coating on pool boiling. In: Experimental Thermal and Fluid Science 35 (2011) 1239-1249
- [12] T. Kim, W. J. Chang, S.H. Chang, Flow boiling CHF enhancement using Al₂O₃ nanofluid and an Al₂O₃ nanoparticle deposited tube. In: International Journal of Heat and Mass Transfer 54 (2011) 2021-2025
- [13] T. Kim, Y.H. Jeong, S.H. Chang, An experimental study of CHF enhancement in flow boiling using Al₂O₃ nanofluid. In: International Journal of Heat and Mass Transfer 53 (2010) 1015-1022
- [14] S. Nishio, H. Tanaka, Visualization of boiling structures in high heat-flux pool-boiling. In: International Journal of Heat and Mass Transfer 47 (2004) 4559-4568

2.0 Boiling Effects of Electrophoretic Deposition of Nanoparticles on Cladding Surfaces

Executive Summary

Bubble dynamics for saturated nucleate boiling at atmospheric pressure for pure water on nanoparticle surface coating on a 0.625mm diameter Zirconium wire have been photographed using a high-speed-camera. Boiling experiments were carried out on the surface modified wires fabricated by the electrophoretic deposition (EPD) process using 60-80nm titanium and 60-80nm titania respectively. Critical heat flux (CHF) enhancements for pool boiling were observed up to 27% for the titanium coatings and 65% for the titania coatings compared to bare Zirconium wires. At 300kW/m² surface heat flux, the nucleate site density on the titanium coating and the titania coating were observed to be 47% and 45% less than the bare wire. In terms of bubble departure volume, the each coating had 16% and 29% smaller volume than the bare surface, respectively. In addition, the average bubble departure frequency of the each coating had 43% and 101% higher than that of the bare case. The nanoparticle surface coatings enhanced the natural and forced convection contribution to the total heat flux, whereas the latent heat contribution was reduced. It is concluded that the chemical property of nanoparticles and the nanostructured surface play an important role in boiling behavior as a function of input power and CHF improvement.

2.1. Introduction

Boiling heat transfer is an effective method in recent energy industries including refrigeration system, high powered electronics, and nuclear reactor to remove high heat fluxes from heated area. The cooling systems usually operate in nucleate boiling regime, which generates rapid small bubbles and allows efficient heat transfer from the surface by latent heat transfer and enhanced local convection. The nucleate boiling, however, is limited by Critical Heat Flux (CHF), where a vapor blanket covers entire heated area and deteriorates heat transfer. Since heated surface would be damaged at CHF due to temperature

excursion, particularly, CHF enhancement is a significant issue in nuclear reactor system to operate in safety margin of boiling water reactor. Pressurize water reactor having higher CHF value also improve economics for electricity generation. Therefore, postponement of CHF phenomena has been investigated extensively by many researchers worldwide, and some trials have mainly focused on surface treatment of a heater. Coating porous media, oxidizing, increasing roughness, and fabricating micro structures on a heated surface can be examples. Moreover, more recent studies on CHF enhancement have been concentrated changing surface conditions by using nanotechnology.

Uniform porous coatings using copper particles (40~80 μ m) on horizontal copper disk heater increased 1.8 times CHF value in pool boiling of distilled water [1]. B.J. Zhang and K. J. Kim [2] observed that three dimensional, interconnected alumina nano porous surface fabricated by an anodic oxidation technique achieved CHF augmentation (108%) and wall superheat reduction compared to untreated surface. Kim et al. [3] fabricated nano-structures and micro scale octagonal posts on silicon-ZnO surfaces by using MEMS technique and the optimal geometry produced 107% in CHF enhancement in water. Also, roughness-augmented surface having micro-pillar arrays fabricated by deep reactive ion etching increased CHF about 160% with water as the working fluid [4]. In addition, nanofluid-deposited porous layers have drawn a great attention to augment CHF. The fact that nanoparticles deposit on a heating surface during nanofluid boiling is widely recognized, and it was proved experimentally that the primary reason of CHF enhancement is not nanofluid itself but the nanoparticle fouled surfaces [5]. C. -K. Huang et al. [6] has reported that TiO₂ nanoparticle coated nickel wire produced by electrical heating in 1wt.% with nanofluid showed up to 82.7% enhancement on CHF in pure water. H. Sakashita [7] also fabricated TiO₂ coated surface on Ni plated copper heating surface by nucleate boiling of TiO₂-water nanofluid. It was found that CHF of water on the coated surface increased up to 1.8 times the CHF for the uncoated surface. Up to now, however, there has been a dispersion of the results of CHF experiments using nanoparticle boiling deposition because boiling deposition process is difficult to control and not well understood [8]. Therefore, few studies have tried to fabricate nanoparticle deposition by means of Electrophoretic

deposition (EPD) technique. The negative charged particles move toward the surface with positive charge, and those form nanoparticle layer on the surface while electrical field is applied between them immersed in nanofluid. The method permits to control the coating thickness by applied voltage, duration, and concentration of nanofluid. S.B White et al. [9] observed 200% improvement in the boiling heat transfer coefficient for deionized water boiling in stainless steel surface with ZnO coating which was fabricated by EPD technique with propylene glycol based nanofluid. In addition, B. Stutz et al. [10] have compared boiling characteristics of vigorous boiling deposition and electrophoresis deposition of maghemite nanoparticles on platinum wire in water. Both coatings increased the CHF and reduced the heat transfer coefficients. The CHF enhancement relied on the covering rate of the heated area.

The mechanism of CHF enhancement by the surface treatments has been believed that changes of physical or chemical properties of the surface such as microstructure, wettability, roughness, capillary force, and porosity give effects on bubble dynamics and liquid motion near heated surface. Therefore, the present work aims to contribute to the understanding of the effects of nanoparticle coating on heated surface and underlying mechanism of CHF enhancement by boiling visualization. The Zirconium thin wire was coated by Titanium (Ti) and Titania (TiO_2) nanoparticles by EPD technique with Acetylaceton based nanofluid, respectively. Each wire was heated by electric joule heating till CHF, and all bubble behaviors were recorded by a high speed camera to analyze bubble departure size, nucleation site density, and bubble departure frequency.

2.2. Experimental Procedure

2.2.1. Preparation of Nanofluid

The two nanoparticle materials, titanium (Ti) and titania (TiO_2), for this study have been selected. Acetylaceton based nanofluid of these two materials were purchased from SS Nano (titanium) and Alfa Aesar (titania). The average diameters of the particles were both 60-80nm from the vendor. The particles were dispersed at concentration of 0.5% by weight with acetylaceton, and minimal addition of

triethanolamine (TEA) to aid in charging the solution and to stabilize the pH. In order to get uniformly suspended nanofluid, a probe sonicator (Misonix 4000) was used to sonicate the mixture for 15 minutes at a frequency of 50Hz. This generated a significant amount of heat in the nanofluid, raising the temperature as high as 50°C, and the temperature of the solution was maintained using a hot plate prior to deposition experiments. The study assumed that various properties such as viscosity, thermal conductivity, and surface tension of the nanofluid with low concentration were not significantly changed according to experimental results from Kim et al [11].

2.2.2. Coating procedure

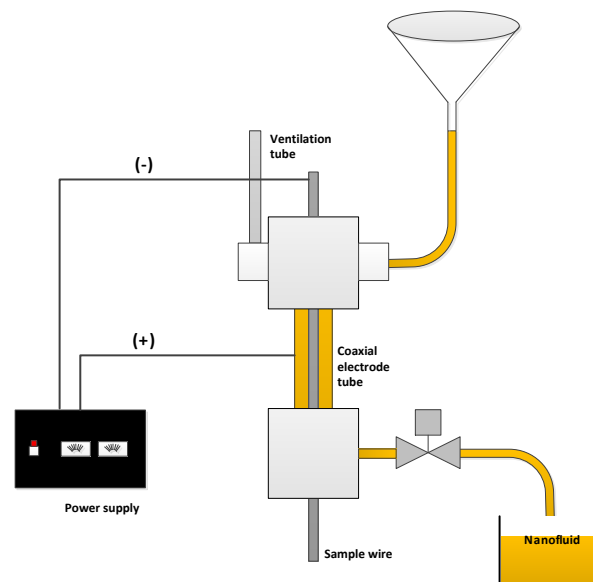


Figure 1 - Schematic view of the co-axial EPD system. Nanofluid from a reservoir fills inside the coaxial electrode tube, and the particles in the solvent are coated on the wire surface at static condition by electrophoretic force.

The Zirconium wires (99.9%) with 0.635mm diameter purchased from ESPI metals were used as a coating substrate, and these were cut 8.5cm long each. To clean the wire surface before making a coating, the sample wires cleaned with distilled water and methanol several times. The samples coated via EPD were placed coaxially within a tungsten tube in a vertical orientation. The tungsten tube and the wire sample acting as electrodes were separated by Teflon blocks and they were connected through wires to a

The boiling behavior of Zirconium wires in distilled pure water was measured in the apparatus in Figure.2, which basically consists of a sample wire submerged in water at atmospheric pressure within Pyrex tank and a large coil heater, and two copper electrodes. The liquid medium was boiled for an additional 10 minutes after the water reached saturation by the coil heater to remove non-condensable gas. Throughout this process, a low-level voltage of approximately 0.2V was applied using DC power supply (DCR20-115B) across the wire to document the change in resistance as the wire was heated. After 10 minutes of boiling the heater was shut off, the zirconium wire started to be supplied power via the copper electrodes gradually. A LabVIEW control automated this ramp so as to increase the power output linearly. The increment of power ramp was controlled to be 0.2W. The experiment concluded when there was a critical heat flux (CHF), immediately after which the wire developed a hot spot and broke. More detail explanation was discussed in our earlier publication [12].

The boiling visualization experiment was carried out to observe bubble dynamics in the boiling experiments. A high speed camera (Motion Pro HS-3) installed with the same boiling experiment apparatus. Four halogen lamps (150W) and a reflected umbrella brightened a window at the horizontal ends of the tank to record pictures clearly. At a given heat flux, bubble dynamics along the heated surface were photographed using the camera. A frame speed of 1000 frames/s has been used in all the experiments. Successive frames were individually viewed and analyzed by image processing software, Image J, to determine the number of active nucleation sites, the bubble departure sizes, and bubble departure frequencies.

2.3. Results

2.3.1. EPD Surface morphology (SEM) and coating thickness

The thickness of EPD coatings of each the wire sample was obtained using SEM images of vertically oriented samples before the boiling experiments. Both of coatings had approximately the order of 4 μm to 6 μm thickness (Figure. 3), so the coating thicknesses are typically only about 1% of the wire diameter.

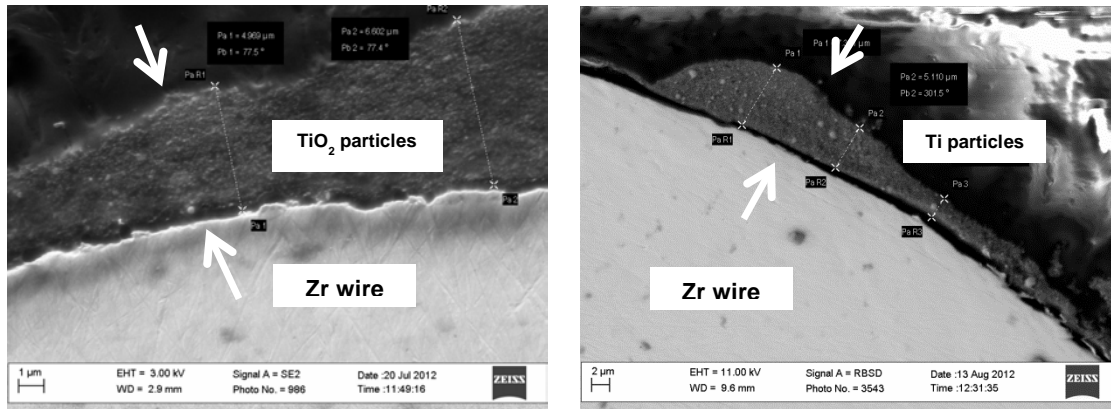


Figure 3 - SEM images showing thickness of 60-80nm titania and titanium EPD coatings on bare Zirconium wire. The light gray portion is the zirconium wire, whereas the darker surrounding indicates the particles.

Figure 4 shows several surfaces of samples: Ti coated surface before boiling (Figure 4(a)), Ti coated surface after boiling (Figure 4(b)), TiO₂ coated surface before boiling (Figure 4(c)), TiO₂ coated surface after boiling (Figure 4(d), (e)), and bare zirconium surface (Figure 4(f)). The particles were deposited dense on the wire samples through EPD process shown in the figure 4 (a) and figure 4 (c). The coatings looked uniform but there were wrinkled structure on the surface, which are repetition of small peak-and-valley structures. The post-CHF image of Ti EPD coatings was observed that there were no changes in coating morphology during the boiling experiment. During the boiling experiments, however, TiO₂ coatings were damaged much, and some part of the nanoparticle coating has been flaked off and left behind a residual surface coating that is dark gray in figure 4 (d). The larger magnification (1kX) of TiO₂ coating revealed that there were lots of micro-cracks on the surface (figure 4 (e)). These coating damages have not been observed on Ti EPD coatings either before or after CHF tests. According to the facts that surface damages were only shown in TiO₂ coating, Ti coating has better adhesion characteristic to the substrate than TiO₂ coatings. This is because the interfacial adhesion strength should be different between metallic coating and metal substrate, and ceramic coating and metal substrate. A post deposition sintering step was found to be necessary in order to consolidate the coating and improve the adhesion of coating to the substrate [13].

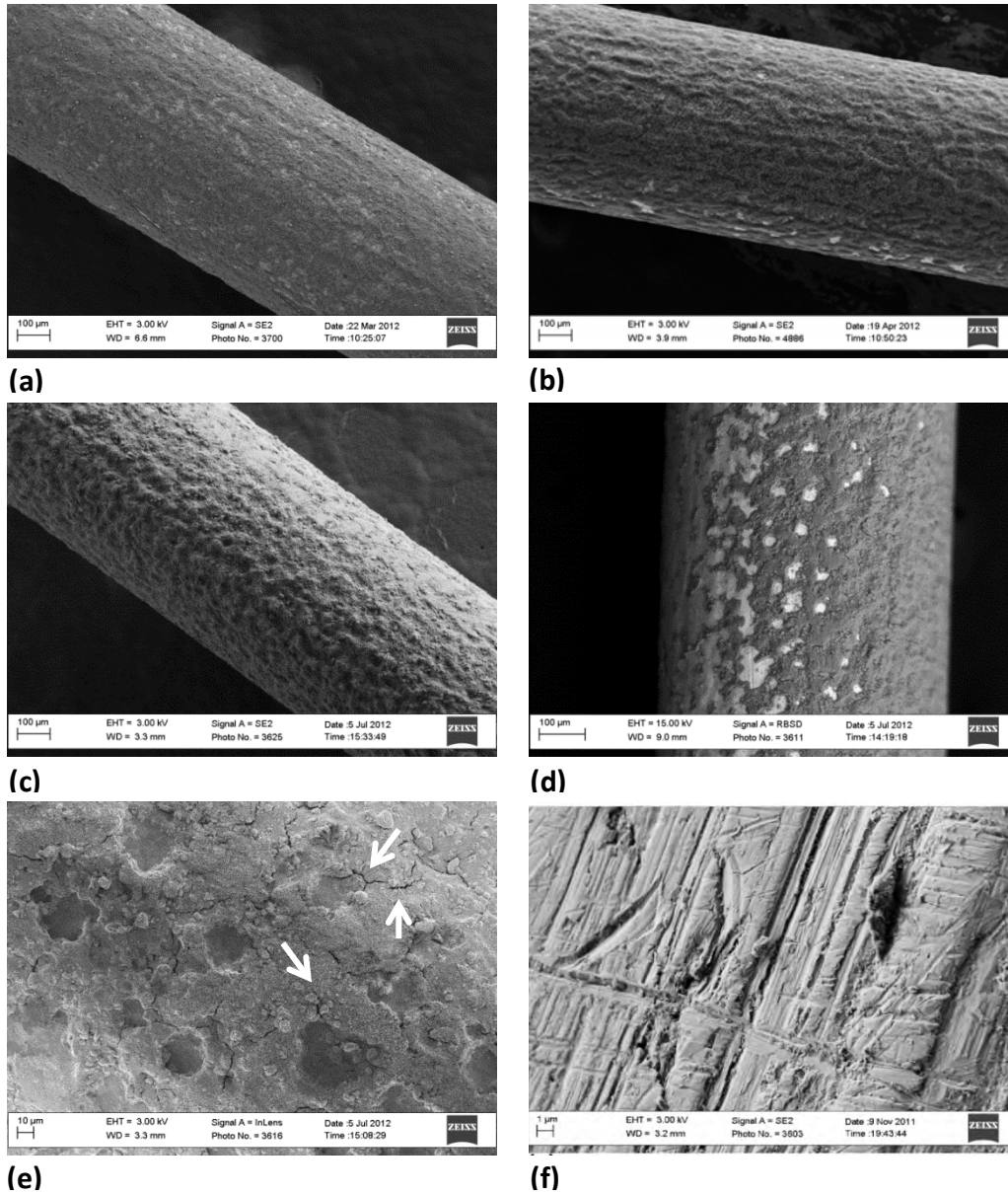


Figure 4 - SEM images of surface of coatings: Ti coated surface before boiling (a), Ti coated surface after boiling (b), TiO₂ coated surface before boiling (c), TiO₂ coated surface after boiling (d) and (e), and bare zirconium surface (f). Both surfaces of Ti and TiO₂ particles seem to be dense, and the samples have wrinkled deposition structures on the surface. However, boiling experiments makes damages only to TiO₂ coatings. Arrows (e) indicate micro-cracks on the surface.

2.3.2. Boiling curve

The boiling curves of bare wire (Figure 5), Ti coated wire, and TiO₂ wires have been obtained by wire surface temperature and calculated heat flux from acquired data. The surface temperature of the wires was evaluated using the temperature coefficient of the resistance method, which temperature changes is correlated to the change in electrical resistance. Electrical resistance data at certain temperature enabled us to figure out the coefficient (α) of bare zirconium wire. The test bare Zr wire was immersed in temperature maintained pure water bath, and it heated with 0.2V increment for 3 temperature set points (20°C, 35°C, and 99°C) for about 2 minutes to measure resistance changes in temperature by using the data acquisition system. The excellent linearity of the responses was observed, and the average value of the calculated coefficients from 3 sets of experiments was used in Figure 5. Moreover, the heat flux through the wire was determined by voltage drop and current across the wire, and total surface area of the wire. The surface superheat and heat flux of the wire can be represented by:

$$\Delta T_{sup} = \frac{R_{sup} - R_{sat}}{R_{sat} \cdot \alpha} \quad (1)$$

$$q'' = \frac{V \cdot I}{A} = \frac{V \cdot I}{\pi \cdot D \cdot L} \quad (2)$$

The uncertainty of $\pm 2.4\%$ on the heat flux resulting from the combined effects of current, voltage, heated length, and wire diameter measurement.

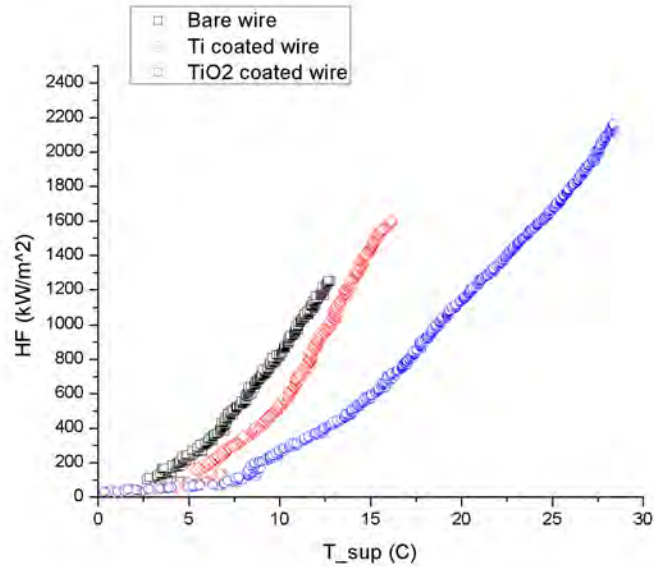


Figure 5 - Boiling curves for 0.625mm Zirconium bare wire in pure water (black dots), wire 60-80nm Ti coated using EPD in pure water (Red dots), and wire 60-80nm TiO₂ coated using EPD in pure water (Blue dots).

The boiling curves indicated that three curves were very similar in natural convection region, which is before the formation of bubbles on the heated surface. The superheat of starting boiling, onset of boiling (ONB), was different from the each surface. Bare wire had the lowest superheat to form the first bubble on the surface near 5°C, but TiO₂ coating needed about 8°C to initiate bubbles. These observations have been also reported from the boiling experiments on a hydrophilic surface conducted by Benoit Stutz et al. [10] and Eric Forrest et al. [14]. In addition, the three boiling curves have shown that boiling incipient hysteresis existed in the boiling developing process. The hysteresis has not been clearly understood but it was hypothesized that the rough or porous surfaces led to the hysteresis [15]. The CHF's obtained from the experiments are seen in Figure 6. 10 samples were boiled to get CHF in each case.

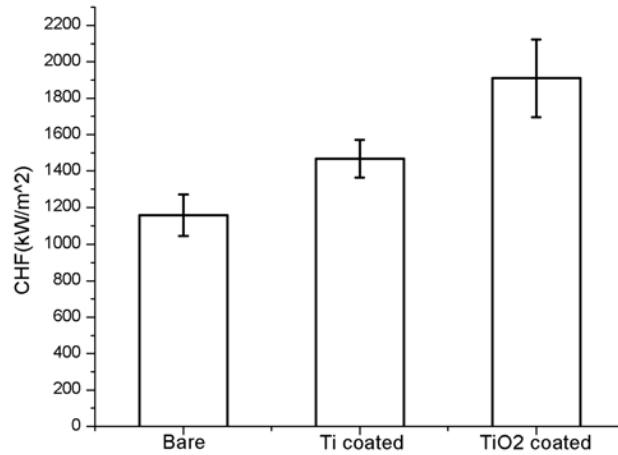


Figure 6 - CHF values for Zirconium wires coated with 60-80nm Ti and TiO₂ by EPD, bare wire.

EPD nanoparticle coated wires showed a significant enhancement in the CHF values compared to those tested in pure water. The TiO₂ coatings and Ti coatings were able to increase CHF about 65%, and 27% respectively. Table 1 also summarizes average CHF values for all boiling test.

Table 3- Summary of CHF results of 0.635mm zirconium wire boiling experiments.

Test case	Average CHF (kW/m ²)	CHF standard deviation (%) [# tests]	CHF enhancement (%)
Zuber correlation	1183	-	-
Bare wire	1157	9.8 [10]	-
60-80nm Ti EPD coated	1468	7.0 [10]	27
60-80nm TiO ₂ EPD coated	1908	11 [10]	65

The CHF value of water is quite consistent with CHF prediction of Zuber correlation [16]:

$$q''_{CHF} = K\rho_g h_{fg} \left[\frac{g\sigma(\rho_f - \rho_g)}{\rho_g^2} \right]^{\frac{1}{4}} \quad (3)$$

The correlation was used 0.16 as the value of constant K. The popular hydrodynamic instability theory cannot explain the CHF enhancement by the nanoparticle coatings. A reasonable explanation for the phenomenon is that Zuber correlation does not account for surface parameters which could affect CHF such as roughness, wettability, geometry, and capillary characteristic of heating surface. Moreover, even though Ti and TiO₂ coatings had almost the same surface structure before the boiling tests, the CHF enhancements of the coatings were distinct remarkably. This implies that micro-structure on the heated surface is not the only reason of the CHF enhancement. In order to observe boiling characteristic of coated surface, the following boiling visualization was carried out.

2.3.4. Bubble dynamics

The boiling visualization experiment expected that the nanoparticle coatings give significant effects on not only CHF value but also bubble dynamics. Recorded images of bubble behaviors enable us to compare bubble departure volume, bubble nucleation site density, and bubble departure frequency of uncoated and coated wires. Lastly, latent heat removal, heat removal mechanism by formation of bubbles, could be evaluated from the combination of the three parameters of bubble dynamics.

2.3.4.1. Bubble departure volume (V_{bubb})

The effect of EPD nanoparticle coating was experimentally examined using images from the high-speed camera. The experiment was conducted with three samples (Bare, Ti coated, TiO₂ coated) submerged in saturated pooling boiling condition. The 500 images containing entire boiling surface were analyzed at certain heat flux. The frame speed was 1000 frames/s, and the bubble behavior was recorded for 0.5 second at each heat flux, and the condition was applied to every boiling experiment. The image recording was carried out till just before CHF, so images of the highest heat flux enabled us to observe bubble

dynamics near CHF. More than 100 bubbles were randomly selected to determine average bubble departure volume. In this study, average bubble departure volume was evaluated instead of average bubble departure diameter because it is difficult to define bubble diameter from the images at high heat flux. The most bubbles were not sphere except for low heat flux ($<100\text{kW/m}^2$). Therefore, we assumed that all bubbles were ellipsoid shown in figure 7.

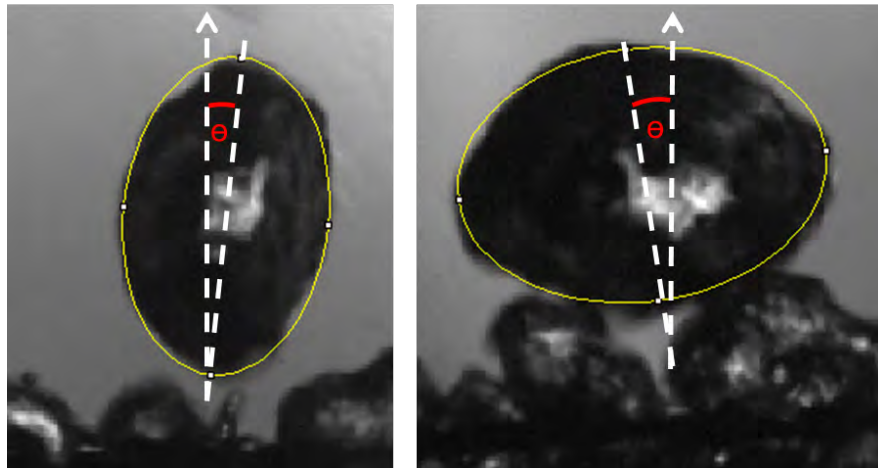


Figure 7 - Bubble images in bare Zr wire at 777kW/m^2 . Shape of most bubbles is ellipsoid according to the images.

The bubbles just departing the wire were analyzed using Image J to get length of major axis and minor axis, and angle deviating from perpendicular to the wire. The angle was used to figure out rotating axis to convert 2D area to 3D volume approximately. Single bubble volume was obtained by rotating the oval using the axis of rotation, and calculated 100 bubbles volumes concluded average bubble departure volume for a given heat flux. If the bubbles combined before leaving the surface, the bubble size was measured a final bubble departing the surface. Therefore, observation of bubble growth history was necessary to figure out a final bubble volume. Base on the pixel resolution and measurement error, the uncertainty in the measured bubble volume was estimated to be $\pm 0.05\text{mm}^3$.

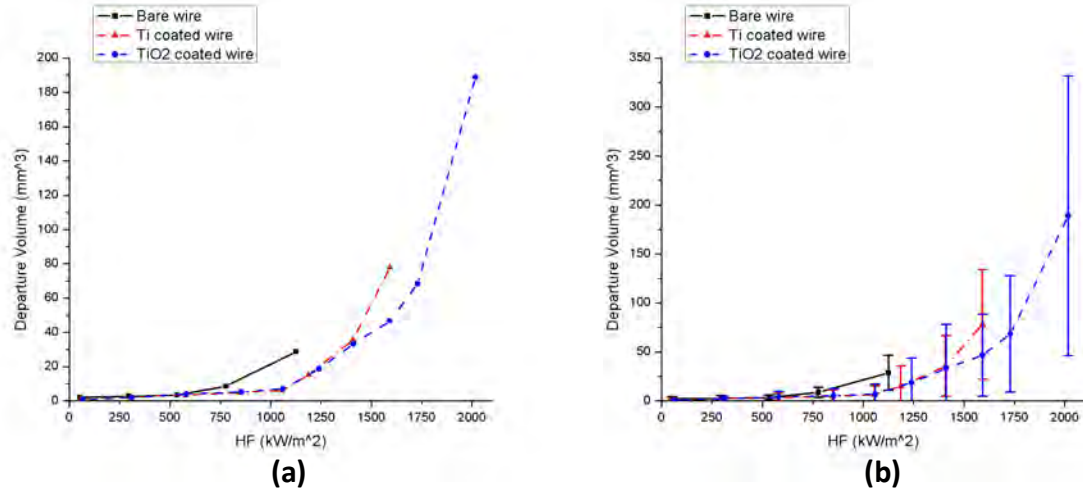


Figure 8 - Bubble departure volume of bare Zr wire (black solid line), Ti coated wire (red dash dots), and TiO₂ coated wire (blue dots) without (a) and with (b) standard deviation.

Figure 8(a) and (b) show average bubble departure volume of each sample with and without standard deviation. The value of average bubble departure volume increases very slowly as the surface heat flux increased, but it increases with large slope when the heat flux approaches its CHF. As seen in the figure 8(a), the three lines are overlapped till about 600 kW/m^2 , and the bubble volume of bare Zr wire starts to deviate from the lines at first, and subsequently Ti coated Zr wire also starts to deviate from the overlapped lines near its CHF. It might be explained from the following. A bubble grows with a certain rate by increasing surface heat flux. However, the fact that bubble blanket forms on heating surface near CHF so bubble merging occurs extensively leads to grow a bubble size suddenly. The largest bubble size was measured near CHF of TiO₂ coated wire. Also, bubble size of bare Zr is larger than that of the coated wires till CHF of bare wire. In addition, the standard deviation gets larger when the wire was applied high heat flux. It implies that sizes of bubbles are relatively uniform at low heat flux but there is broad size distribution of bubbles at high heat flux due to bubble coalescence.

2.3.4.2. Nucleation site density (N)

To evaluate nucleation site density, 18 images with 0.03s time interval were analyzed and made it arithmetic average. The number of bubbles attaching on the entire heated wire in each image was counted

by using the image processing software, and a large bubble formed by bubble coalescence was counted as a single bubble. Total number of bubbles was divided by length of wire recorded to get the site density. Since an active nucleation site was observed to be inactive occasionally and some inactive surface suddenly started to form a bubble, it is concluded that a bubble nucleation is a stochastic event. Moreover, the most individual nucleation site behaves independently of each other. A bubble nucleation site density is changed with surface heat flux and heated wire condition. The average site density of the three cases increased with increasing surface heat flux till a certain heat flux value. After then, the site density decreased, thus minimum nucleation site density occurred at CHF (see Figure 9). From the images, small bubbles were nucleated on the wire without touching each other at low heat flux, however, with increased heat flux, the entire surface of wire was fully crowded with a large number of bubbles, and the bubbles started to combine each other immediately when they touched. Therefore, large volume bubbles could be generated due to bubble merging, and it gave rise to reduce nucleation site density.

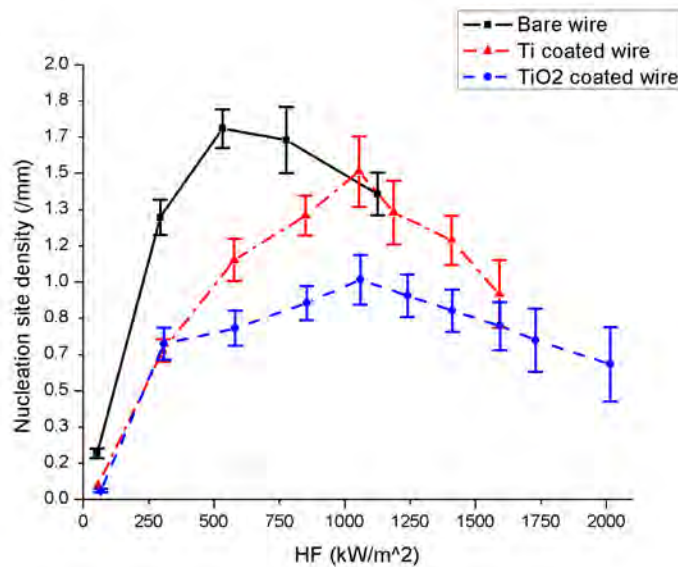


Figure 9 - Bubble nucleation site density of bare Zr wire (black solid line), Ti coated wire (red dash dots), and TiO₂ coated wire (blue dots) in each heat flux.

Interestingly, bubble nucleation site density has been reported as the linear relationship with surface heat flux by D.D Paul et al. [17] using platinum wire in pure water pool boiling experiment, which is a contrast to our results. This is because that the plots in Figure 9 account for bubble coalescence phenomenon but D.D Paul's study only focused on the number of isolated bubbles. Moreover, heat flux region of the experiment were narrow ($<600\text{kW/m}^2$) so it is hard to observe bubble dynamics near CHF. In addition, as shown in figure 10, the number of bubbles on bare Zr wire is about 47% and 45% larger than that of Ti and TiO_2 coated wire in 300kW/m^2 surface heat flux, respectively. The result also could be confirmed in Figure 9.

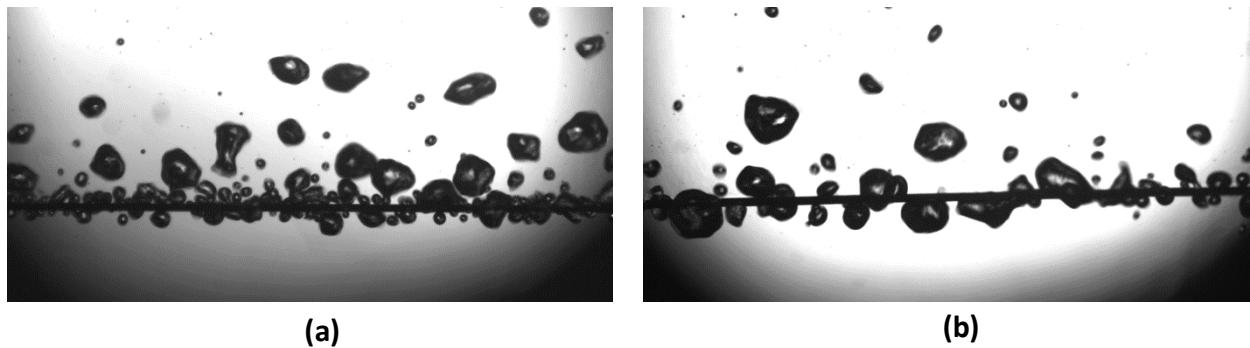


Figure 10 - Images of boiling on entire bare Zr wire (a), and TiO_2 coated wire (b) at 532kW/m^2 and 581kW/m^2 , respectively. The number of bubbles on the wire is different between the cases at a glance.

At all heat fluxes, the coated wire had less bubble nucleation site density than the bare wire except for heat flux near CHF of bare wire. It means that the nanoparticle coatings had a lower heat transfer coefficient, in other words, their wall superheats were greater than that of the bare wire. The boiling curve in figure 5 can also make sure the result. Since less nucleation site density in boiling was observed in super-hydrophilic coating surface condition [14], it is possible to think that Ti and TiO_2 coatings had also hydrophilic characteristics. Moreover, It is interesting to note that the Ti and TiO_2 coatings showed the similar number of bubble nucleation site at low heat flux ($<400\text{kW/m}^2$) but TiO_2 coatings had less bubble formation on the surface above the heat flux. There was not much difference of thickness and particle size of two coatings, and the surface morphology had no significant differences each other. Therefore,

chemical properties such as wettability and capillary force might change the bubble nucleation site density.

2.3.4.3. Bubble departure frequency (f)

The bubble departure frequency could be estimated by counting the number of frames between consecutive bubble departures. The number of frames including bubble waiting period and bubble growth to its departure diameter were divided by frame rate (1000frames/s) to get time period. By definition, bubble departure frequency is determined using time period as follows:

$$f = \frac{1}{t_{wa} + t_{gr}} \quad (4)$$

100 bubble nucleation sites were randomly selected in an entire wire to obtain a statistically significant measurement of the frequency. The uncertainty of the bubble departure period was estimated to be within 0.001s, which was time between two sequential frames.

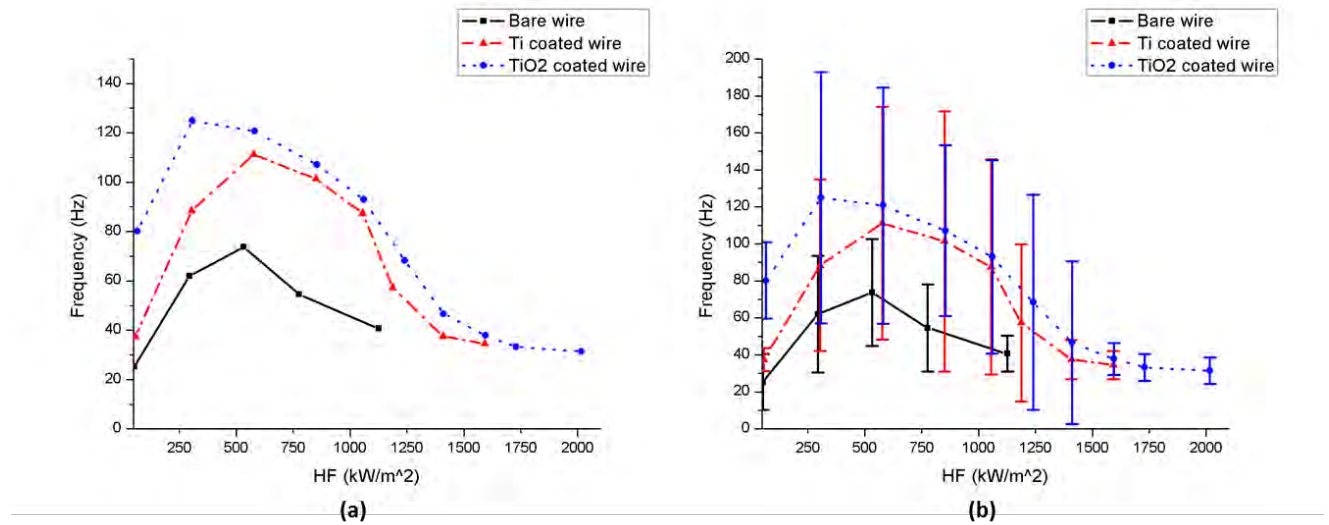


Figure 11 - Bubble departure frequency of bare Zr wire (black solid line), Ti coated wire (red dash dots), and TiO2 coated wire (blue dots) without (a) and with (b) standard deviation.

The observed average bubble departure frequencies are plotted at each heat flux in Figure 11. Bubble departure frequencies of the coated wires were always larger than those of bare Zr wire at each surface heat flux. Ti and TiO₂ coated wires augmented 43% and 101% of bubble departure frequency compared to bare Zr wire at 300kW/m². Moreover, similar to the nucleation site density, the average bubble departure frequency increased as the boiling heat flux increased till a certain heat flux, and the frequency decreased after the point. Bubble departure on the heated surface was delayed owing to bubble coalescence, and two major mechanisms of bubble coalescence were observed from the images. Firstly, small bubbles from distinct nucleation sites contribute to form a large bubble before departing from the surface. Secondly, individual bubbles periodically generated from a single nucleation site make a large bubble. The two mechanisms are shown in figure 12.

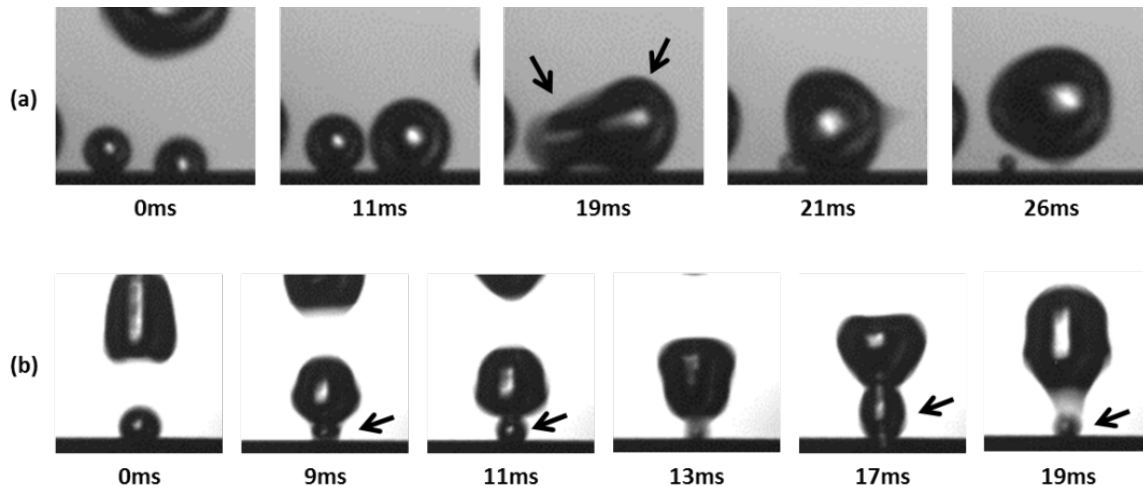


Figure 12 - Bubble growing and coalescence (a) bare Zr wire at 52.6kW/m² and (b) TiO₂ coated Zr wire at 66.7kW/m² in pure water. Black arrows refer bubbles combining each other (a) and new bubble generated just below the former bubble.

As seen in figure 12, bubble coalescences occurred on the wire although there was a low heat flux region (~60 kW/m²). Since bare Zr wire has more bubble nucleation sites than coated wires, there are more chances for bubbles to contact each other. For example, two bubbles combined immediately and form a larger bubble (figure 12 (a)), after two bubbles contact each other. In terms of the nanoparticle coated wires, a bubble mainly tended to stay on the surface by the latter type of bubble coalescences due to a

large bubble growth rate and small waiting time. A new bubble (black arrows in figure 12 (b)) generated beneath the original bubble even though former had not departed yet, and finally 4 bubble coalescences were observed until a bubble departure. Therefore, the two ways of bubble coalescence surely cause a vapor layer formation at high superheated surface, and finally lead to CHF. Plus, large uncertainties at intermediate heat flux region (figure 11 (b)) was attributed to frame rate of the camera.

2.4. Discussion

2.4.1. Latent heat contribution

Experimental data for the average bubble departure volume, the average nucleation site density, and the bubble departure frequency allow us to examine latent heat contribution in total heat flux. The total heat flux from the heated wire above saturation temperature to water consists of natural convection, force convection, and latent heat by bubble formation as shown equation (5).

$$q''_{TOT} = q''_{CV} + q''_{LT} = q''_{NC} + q''_{FC} + q''_{LT} \quad (5)$$

Rohsenow [18] postulated that heat flows from the surface first to the adjacent liquid, as in any single-phase convection process, and heat also transfer to liquid remarkably by local agitation due to liquid convective flowing behind the wake of departing bubbles. Thus, heated wire surface without bubbles in the images accounts for heat transfer by liquid convection. Moreover, the heat transfer to a bubble while attached to the wire surface is given by

$$q''_{LT} = \frac{\rho_g h_{fg}}{\pi D_W} \langle V \rangle \langle N \rangle \langle F \rangle \quad (6)$$

where $\langle V \rangle$ is the average bubble departure volume, $\langle N \rangle$ is the average number of nucleation sites per unit length, and $\langle F \rangle$ is the average bubble departure frequency. Vapor density (ρ_g) and the enthalpy difference (h_{fg}) of pure water were determined at atmospheric pressure. The result of the calculation is plotted in Figure 13.

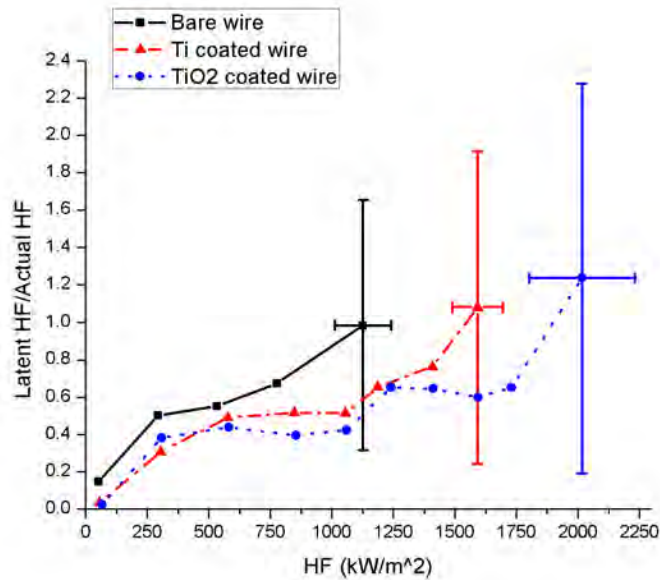


Figure 13 - Relative latent heat flux contributions for boiling experiments with bare Zr wire (black solid line), Ti coated wire (red dash dots), and TiO₂ coated wire (blue dots).

As the applied heat flux in a wire increased, the ratio of latent heat to total heat flux became significantly important in both uncoated and coated Zr wire samples. The latent heat flux contribution reached about 100% of the total heat flux as CHF approached. In other words, heat transfer contribution by fluid convection is dominated in low heat flux region but its portion vanishes near CHF. It is interesting to note that latent heat contribution of the coated Zr wires was always smaller than that of bare Zr wire, primarily, owing to reduction of active nucleation sites. For instance, at 800kW/m² surface heat flux, for example, latent heat contribution to the total heat of bare wire, Ti coated wire, and TiO₂ coated wire was 68%, 52%, and 40%, respectively. The nanoparticle coatings allowed the heated wire to dissipate heat without bubble formation through enhanced convective heat transfer. Enlarged surface area by the coatings might give positive effects on natural convection, and forced convection can be augmented by agitation of the thermal boundary layer in the vicinity of bubble nucleation sites due to the fast bubble growth and departure from the coated surfaces. Also, Ti and TiO₂ coated wire have a similar trend of the ratio, but latent heat contribution of Ti coated wire reached 100% of the total heat flux at lower heat flux compared to TiO₂ coated wire case. Moreover, there were sudden increases of the latent heat contribution just before

CHF, and the phenomenon is mainly caused by the formation of abnormally large bubbles near CHF. Error bars of x direction represent CHF variation in 10 experiments, and the latent heat ratio uncertainty is shown in error bars of y direction.

2.4.2. The mechanism of the bubble dynamics

The effects of Ti or TiO₂ nanoparticle surface coating in boiling behaviors can be summarized as following: Delayed ONB, CHF enhancement, bigger bubble departure size, less bubble nucleation site, and higher bubble departure frequency.

Most studies have tried to explain CHF enhancement in nanoparticle coated surfaces by measurement of static contact angle (θ) [2,3,7,9-11,14,19], and the nanoparticles or nanostructure surface modification have shown high wettability characteristics observed as low contact angles. According to the studies, hydrophilic surfaces ($\theta < 90^\circ$) induced higher CHF but slightly lower heat transfer coefficient in nucleate boiling compared to hydrophobic surfaces ($\theta > 90^\circ$). In addition, SiO₂ hydrophilic surface experienced relatively longer natural convective boiling regime with delayed ONB, so the hydrophilic surface degraded heat transfer performance in low heat flux regime [20]. In terms of departure bubble size, Fritz's proposed the following equation [21], which represents that bubble diameter decreases with decreasing contact angle.

$$D_b \sim \theta \sqrt{\frac{\sigma}{g(\rho - \rho_g)}} \quad (7)$$

Also, Y. Nam et al. [22] observed 2.5 times smaller bubble departure diameter and 4 time shorter bubble growth period in water on CuO nanostructured on a silicon substrate with an isolated micro-cavity. The modified surface was proven to be super-hydrophilic surface ($\theta \sim 7.5^\circ$). It is hypothesized that better wettability with higher capillary force bringing fluid near surface to active nucleation sites more effectively, so total bubble period can be reduced [23]. For nucleation site density, hydrophilic surface fabricated by SiO₂ nanoparticle thin film coating produced less nucleation site density in water boiling

compared to bare heated Nickel wire [14]. Moreover, Wang and Dhir [24] suggested that the nucleation site density decreases with contact angle decreasing at given wall superheat or cavity diameter (D_c) as shown in equation (8).

$$N_a = 5 \times 10^{-27} \frac{(1 - \cos(\theta))}{(2D_c)^6} \quad (8)$$

Interestingly enough, boiling heat transfer characteristics including bubble dynamics of Ti and TiO₂ nanoparticle coated surface in our experiments are in agreement with the mentioned researches. Therefore, it is concluded that Ti or TiO₂ nanoparticle coatings can be considered as good wettability surface. However, unfortunately, it is difficult to explain that hydrophilic characteristic of the coating is the only reason of CHF enhancement because other surface factors are also typically coupled with boiling phenomena. As seen figure 3 and 4, the porous layer with micron order of thickness and nano-micro structure on the coated surfaces might give positive effects on CHF enhancement. Moreover, water absorption by capillary wicking on nanoparticle coated surface might also augment CHF in water [25].

2.5. Conclusion

The nanoparticle coated surface effects on bubble dynamics has been studied using boiling visualization. Nanoparticle deposition on thin Zr wire from Ti and TiO₂ nanofluids carried out by the electrophoretic deposition method. The results of bubble dynamics observation from three different conditions (bare, Ti, and TiO₂) at various heat fluxes were compared by obtained images from high speed camera. Based on the results of this investigation, conclusions are the following:

- Nanoparticle layer (Ti or TiO₂) with 4-6 μm thickness was successfully coated on Zr thin wire by EPD technique. Ti nanoparticle coating was more mechanically durable than TiO₂ nanoparticle coating after the boiling experiments.

- Both nanoparticle coated wire delayed ONB compared to bare wire so the surfaces required more surface superheat to initiate bubble, and CHF enhancements of TiO₂ and Ti coated wire were measured about 65% and 27%, respectively.
- Bubble dynamics in distilled water was significantly affected by the nanoparticle coated surface. The presence of the coatings reduced the average bubble departure volume and nucleation site density, and increased bubble departure frequency. Since other researches about boiling characteristics with hydrophilic heated surface have shown very similar results with our study, the coated surfaces can be considered as good wettability surfaces.
- The nanoparticle coatings enabled to reduce latent heat contribution to the total heat flux over all heat flux values, primarily, due to the reduction of bubble nucleation sites. Enhanced convective heat transfer by enlarged surface area and liquid agitation by rapid bubble cycle seems to handle large portion of heat from the surface till CHF.

2.6 References

- [1] G.-S. Hwang, M. Kaviany, Critical heat flux in thin, uniform particle coatings, *International Journal of Heat and Mass Transfer*, 49, 2006, 844-849
- [2] B. J. Zhang and K. J. Kim, Effect of liquid uptake on critical heat flux utilizing a three dimensional, interconnected alumina nano porous surfaces, *Applied Physics Letters*, 101, 054104, 2012
- [3] S. Kim et al, Effects of nano-fluid and surfaces with nano structure on the increase of CHF, *Experimental Thermal and Fluid Science*, 34, 2010, 487-495
- [4] Chu et al, Structured surfaces for enhanced pool boiling heat transfer, *Applied Physics Letters*, 100, 241603, 2012
- [5] H. Kim et al, Effect of nanoparticles on CHF enhancement in pool boiling of nano-fluid, *International Journal of Heat and Mass Transfer*, 42, 2006, 2003-2013
- [6] Chen-Kang Huang et al, Boiling enhancement by TiO₂ nanoparticle deposition, *International Journal of Heat and Mass Transfer*, 54, 2011, 4895-4903
- [7] H. Sakashita, CHF and near-wall boiling behaviors in pool boiling of water on a heating surface coated with nanoparticles, *International Journal of Heat and Mass Transfer*, 55, 2012, 7312-7320
- [8] R.A. Taylor et al, Pool boiling of nanofluids: comprehensive review of existing data and limited new data, *International Journal of Heat and Mass Transfer*, 52, 2009, 5339-5347
- [9] S. B. White et al, Boiling surface enhancement by electrophoretic deposition of particles from a nanofluid, *International Journal of Heat and Mass Transfer*, 54, 2011, 4370-4375
- [10] B. Stutz et al, Influence of nanoparticle surface coating on pool boiling, *Experimental Thermal and Fluid Science*, 35, 2011, 1239-1249
- [11] S.J. Kim et al. Surface wettability change during pool boiling of nanofluids and its effect on critical heat flux, *International Journal of Heat and Mass Transfer* 50, 2007, 4105-4116
- [12] G. Stange et al, A Study of Nanoparticle Surface Modification Effects on Pool Boiling Critical Heat Flux, *Nuclear Technology*, 2012, accepted
- [13] V. Firouzdar et al, Development of Diffusion Barrier Coatings for Mitigation of Fuel-Cladding Chemical Interactions, *Key Engineering Materials*, 2012, accepted

- [14] E. Forrest et al, Augmentation of nucleate boiling heat transfer and critical heat flux using nanoparticle thin-film coatings, *International Journal of Heat and Mass Transfer* 53, 2010, 58-67
- [15] M. Shi et al, Analysis on hysteresis in nucleate pool boiling heat transfer, *International Journal of Heat and Mass Transfer*, 36, 1993, 4461-4466
- [16] N. Zuber, Nucleate boiling. The region of isolated bubbles and the similarity with natural convection, *International Journal of Heat and Mass Transfer* 6, 1963, 53-78
- [17] D.D. Paul et al, A statistical analysis of saturated nucleate boiling along a heated wire, *International Journal of Heat and Mass Transfer*, 26, 1983, 509-519
- [18] W. Rohsenow, A method of correlating heat transfer data for surface boiling of liquid, *Trans. ASME*, 84, 969, 1962
- [19] J. S. Coursey and J. Kim, Nanofluid boiling: The effect of surface wettability, *International Journal of Heat and Fluid Flow*, 29, 2008, 1577-1585
- [20] H. Jo et al, A study of nucleate boiling heat transfer on hydrophilic, hydrophobic and heterogeneous wetting surface, *International Journal of Heat and Mass Transfer*, 54, 2011, 5643-5652
- [21] I.L. Pioro et al, Nucleate pool-boiling heat transfer. I: Review of parametric effects of boiling surface, *International Journal of Heat and Mass Transfer*, 47, 2004, 5033-5044
- [22] Y. Nam et al, Single bubble dynamics on a superhydrophilic surface with artificial nucleation sites, *International Journal of Heat and Mass Transfer*, 54, 2011, 1572-1577
- [23] T.J. Hendricks et al, Enhancement of pool-boiling heat transfer using nanostructured surfaces on aluminum and copper, *International Journal of Heat and Mass Transfer*, 53, 2010, 3357-3365
- [24] C.H. Wang and V.K. Dhir, Effect of surface wettability on active nucleation site density during pool boiling of water on a vertical surface, *Journal of Heat Transfer*, 115, 1993, 659-669
- [25] H.S. Ahn et al. The effect of water absorption on critical heat flux enhancement during pool boiling, *Experimental Thermal and Fluid Science*, 42, 2012, 187-195

3.0 Oxidation Studies of EPD coated Zircaloy-2

The goal of this work was to observe the oxidation prevention of zircaloy-2 and zircaloy-4 provided by electrophoretic depositions (EPD) of nanoparticles that had been examined in critical heat flux experiments (CHF) previously discussed. An optimized protective coating against oxidation was the initial goal of this work. This oxidation and corrosion was to be tested within the UW Engineering Physics critical water loop using zircaloy-4 samples fabricated to be held within a ladder apparatus inside the loop. Several prerequisites had to be met before performing corrosion tests within the loop.

1. The coating to be tested must provide a critical heat flux enhancement to zirconium wires
2. The coating must be between 3-5 microns for reasons including thermal insulation effects, reproducibility, and material bonding.
3. The coating must remain intact proceeding air corrosion studies to mitigate the chances of flaking and contamination during super critical water loop testing.

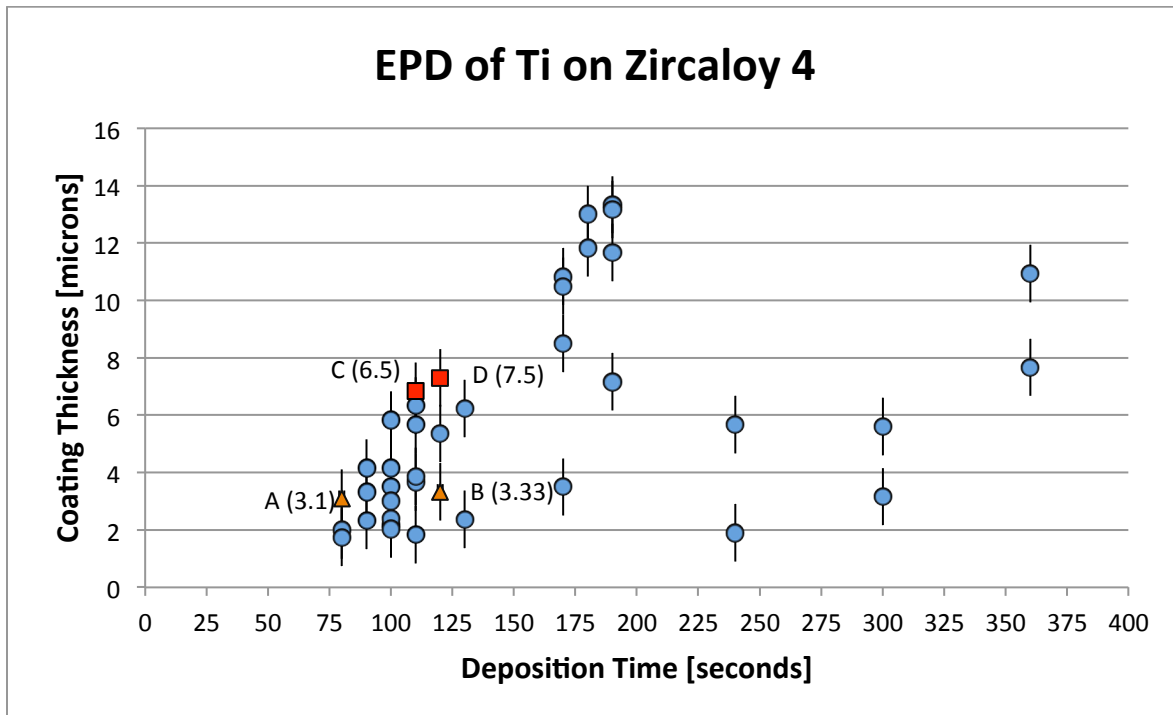
3.1 Coating Selection

Three coatings were selected for corrosion testing. At the beginning of the corrosion studies, titanium coatings had proven to be quite adherent to T-91 steel substrate. CHF experiments had also shown a benefit from this coating on zirconium wire substrate. Additionally, scratch tests performed on T-91 samples after heat-treating the coatings demonstrated an intermetallic bond that secured the Ti coating to the substrate. Yttria-oxide (Y₂O₃) had also been chosen for the study due to its high CHF enhancement. The highest improvements in CHF (210%) were observed when Y₂O₃ was applied to stainless steel wires. Finally, titania (TiO₂) was selected for study because it provided a high CHF improvement on zirconium wires (180%) and had shown good adherence to T-91 steel substrates.

3.2 Deposition

As the three coatings selected (Ti, Y2O3, TiO2) had met the first requirement of enhancing CHF on zirconium wires, the second requirement of 3-5 micron thicknesses had to be achieved. What followed was a series of electrophoretic deposition experiments to observe the necessary parameters for a 3-5 micron deposition. Depositions were on .5'' by .5'' plates of 1 mm thickness. Thickness of coatings was measured using 2 independent methods. A thickness gage with 1 micron resolution and error was used in the first method by taking the average of 3 recordings. The second method used a set of assumptions to calculate the average surface thickness based upon weight change after deposition. Coatings that were within the 3-5 micron range were examined further. Insufficient coatings were cleaned from the substrate for future trials. The graph below demonstrates the variable thickness of titanium coating on zircaloy.

Figure 1: EPD Coating Deposition Thickness as a function of the EPD Deposition Time



As shown, deposition thickness was difficult to replicate when holding all controllable variables constant during the EPD process. Deposition times of 80 to 120 seconds yielded desired coating thicknesses the most consistently within the time range examined.

3.3 Heat Treatment

Samples A and B were tested for their adhesion. B was sintered in a vacuum furnace. Temperature was held at 800 C for 2 hours followed by 950 C for 4 hours. This was done to condense the coating and diffuse it within the substrate to increase adherence. Scratch testing was conducted after sintering. The images below compare a 3.3 micron thick coating that has been sintered (sample B) to a 3.1 micron thick coating as deposited (sample B). The scratch was made with a 150 g weight.

Figure 2: Sample B Image of a EPD Coated Surface (Sintered)

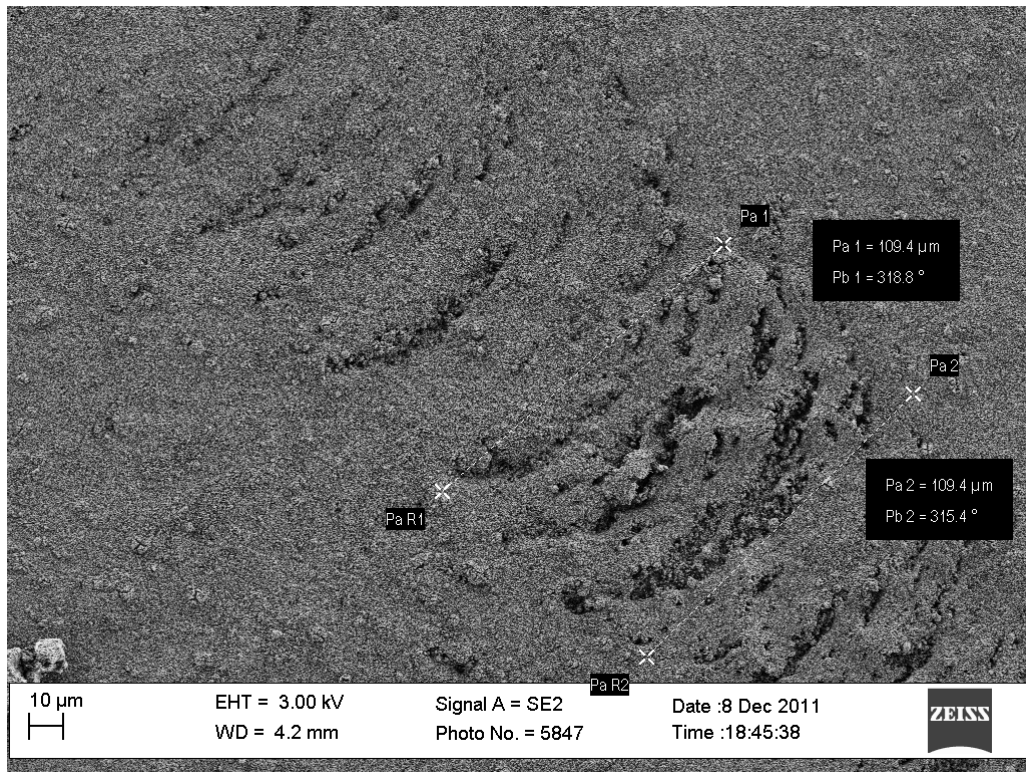
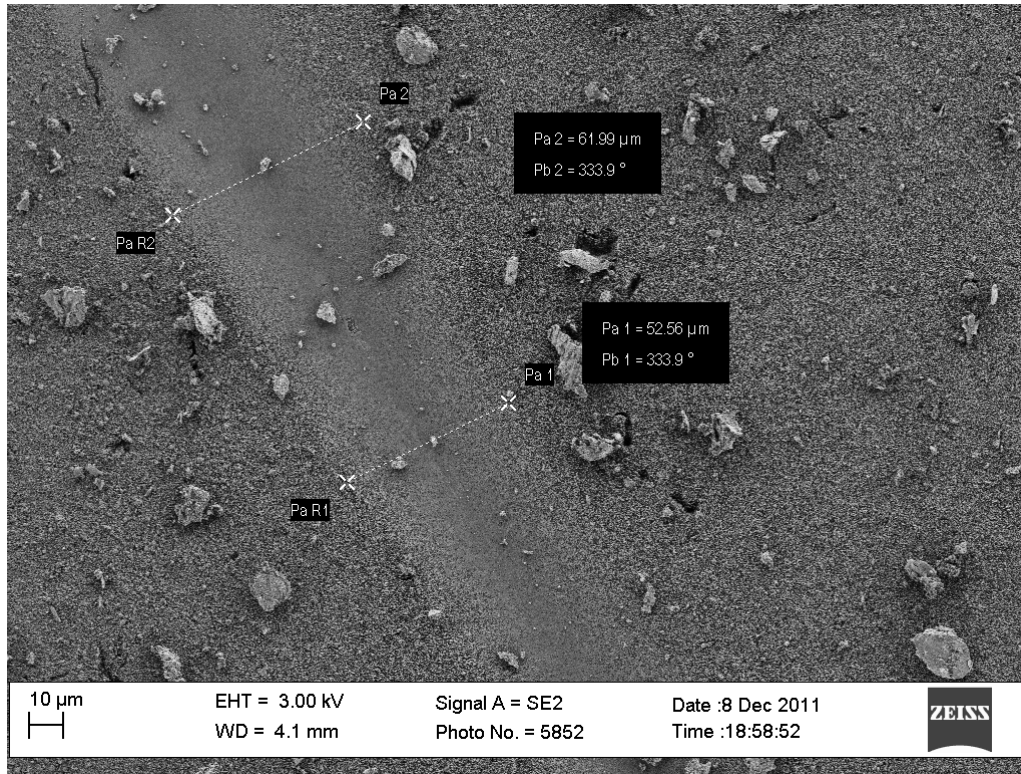


Figure 3: Sample B Image of a EPD Coated Surface (Non-Sintered)

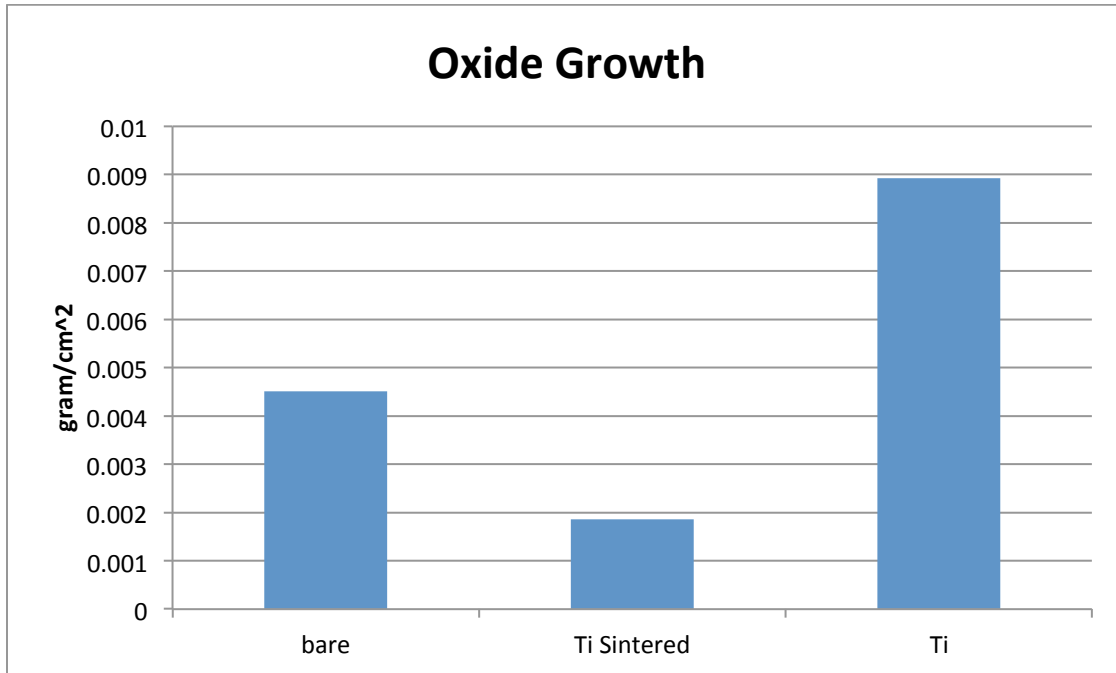


The trough widths produced with the 150 g weight were ~109 microns and ~53 microns for the sintered and non-sintered sample. Thus, the non-sintered sample was more resistant to surface deformation.

3.4 Oxidation Prevention

An additional 2 samples (C and D) had been selected for oxidation testing. Thicker coatings had been selected than for the scratch testing. Despite wider scratch troughs from the sintered samples, it was shown that sintered samples significantly reduced oxide growth of the substrate beneath the EPD coating. The graph below depicts data from 3 samples after oxidation. Oxidation occurred in an open atmosphere furnace for 100 hours at 500 C. The bare sample was simply oxidized with no coating. The sintered sample (D) had a Ti coating of 7.5 microns before being heat treated and then oxidized. The third sample (C) was deposited with a 6.7 micron coating of Ti and was then oxidized. Oxidation of the sintered sample was lower than the other 2 samples.

Figure 3: Comparison of Oxide Growth between Various Sample (with and w/o EPD)



Oxide growth was measured using a thickness gage. There is no discrimination between titanium oxide growth and the zircaloy substrate oxide growth. Focused Ion Beam cross sections were taken to examine the oxidation effects further. This comparison has been made between the sintered sample and bare zirconium sample after oxidation. Bare zirconium had oxidized to a depth of 8-9 microns. The Titanium sintered sample had oxidized to a depth of 3-5 microns. Additionally, there were fewer cracks within this oxidized region. EDS line scans confirm the depths of oxidation.

Though the coating of titanium on zircaloy is extremely variable, protection against oxidation is provided after heat treatment. Heat treatments had been attempted under Argon gas cover and open atmosphere. However, hydriding and heavy oxidation occurred in both these cases. A well adhering coating is still desired for water loop oxidation testing. Adjusting coating thickness and heat treatment may provide this effect. Shortly after acquiring this data, the vacuum furnace ceased operating. Sintering could no longer be performed on titanium samples.

